LEVEL III (14) SDAC-TR-77-7-VOL-1

Vol 2 A084770

(12)

(6)

A COMPARISON OF TELESEISMIC P WAVE AMPLITUDES AND SPECTRA OBSERVED AT SELECTED BASIN AND [redacted] STES AND IN EASTERN NOR[redacted]ERICA. PHASE 1. FINAL REPORT - VOLUME 1.

(9) Final rept.,

(10) Z.A. Der, M.S. Dawkins, T.W. McElfresh, J.H. Goncz, C.E. Gray & M.D. Gillispie
Seismic Data Analysis Center
Teledyne Geotech, 314 Montgomery Street, Alexandria Virginia 22314

(11) 30 May 1978 (12) 87

APPROVED FOR PUBLIC RELEASE; DISTRIBUTION UNLIMITED.

Sponsored by

The Defense Advanced Research Projects Agency (DARPA)

(15) F08606-78-C-0007; DARPA Order No. 2551

Monitored By

AFTAC/VSC

312 Montgomery Street, Alexandria, Virginia 22314

Disclaimer: Neither the Defense Advanced Research Projects Agency nor the Air Force Technical Applications Center will be responsible for information contained herein which has been supplied by other organizations or contractors, and this document is subject to later revision as may be necessary. The views and conclusions presented are those of the authors and should not be interpreted as necessarily representing the official policies, either expressed or implied, of the Defense Advanced Research Projects Agency, the Air Force Technical Applications Center, or the US Government.

Unclassified

SECURITY CLASSIFICATION OF THIS PAGE (When Data Entered)

REPORT DOCUMENTATION PAGE	READ INSTRUCTIONS BEFORE COMPLETING FORM
1. REPORT NUMBER: SDAC-TR-77-7 / 2. GOVT ACCESSION NO.: AD-A085014	3. RECIPIENT'S CATALOG NUMBER:
4. TITLE (and Subtitle): A COMPARISON OF TELESEISMIC P WAVE AMPLITUDES AND SPECTRA OBSERVED AT SELECTED BASIN AND RANGE SITES AND IN EASTERN NORTH AMERICA, PHASE 1 FINAL REPORT - VOLUME 1	5. TYPE OF REPORT & PERIOD COVERED: Technical
	6. PERFORMING ORG. REPORT NUMBER:
7. AUTHOR(s): Z. A. Der, M. S. Dawkins, T. W. McElfresh, J. H. Goncz, C. E. Gray, and M. D. Gillispie	8. CONTRACT OR GRANT NUMBER(s): F08606-78-C-0007 /
9. PERFORMING ORGANIZATION NAME AND ADDRESS: Teledyne Geotech / 314 Montgomery Street, Alexandria, Virginia 22314	10. PROGRAM ELEMENT, PROJECT, TASK AREA & WORK UNIT NUMBERS: VT/7709
11. CONTROLLING OFFICE NAME AND ADDRESS: Defense Advanced Research Projects Agency, Nuclear Monitoring Research Office, 1400 Wilson Blvd., Arlington, Virginia 22209	12. REPORT DATE: 5/30/78
	13. NUMBER OF PAGES: 87
14. MONITORING AGENCY NAME & ADDRESS (if different from Controlling Office): VELA Seismological Center, 312 Montgomery Street, Alexandria, Virginia 22314	15. SECURITY CLASS. (of this report): Unclassified
	15a. DECLASSIFICATION DOWNGRADING SCHEDULE:

16. DISTRIBUTION STATEMENT (of this Report)

APPROVED FOR PUBLIC RELEASE; DISTRIBUTION UNLIMITED.

17. DISTRIBUTION STATEMENT (of the abstract entered in Block 20, if different from Report)

18. SUPPLEMENTARY NOTES

Author's Report Date 07/07/77

19. KEY WORDS (Continue on reverse side if necessary and identify by block number)

ATTENUATION

BODY WAVE MAGNITUDE (m_b)

CRUSTAL AMPLIFICATION

20. ABSTRACT (Continue on reverse side if necessary and identify by block number)

Three Seismic Data Collection System (SDCS) stations were deployed at the Nevada Test Site (NTS) and two in the Eastern United States (EUS) to measure magnitude residuals and spectral differences between NTS and EUS stations. The deployment was intended to determine the degree of anelastic attenuation under NTS. At the Climax Stock (OB2NV) station, the teleseismic body-wave magnitudes are .17 magnitude units (m.u.) lower than at the EUS stations. The magnitudes at the two Pahute Mesa sites are about .2 m.u. higher that at OB2NV,

DD FORM 1 JAN 73 1473 EDITION OF 1 NOV 65 IS OBSOLETE

Unclassified

SECURITY CLASSIFICATION OF THIS PAGE (When Data Entered)

a difference that can be accounted for by amplification of low velocity volcanics under Pahute Mesa. Thus local geology must be taken into account in order to evaluate the attenuation under a given site using amplitude data. This correction shows that with respect to corrected amplitude levels OB2NV is equivalent to Pahute Mesa stations. At all NTS sites the higher frequency content of P waves is significantly less than in the EUS. Available data suggests an attenuation effect of about .2 m.u. under NTS. Measurements at a few other Western United States (WUS) sites, including the site of the SHOAL explosion, yield similar figures. These results confirm that body-waves suffer considerable anelastic losses traversing the mantle under the WUS, including the NTS sites.

A COMPARISON OF TELESEISMIC P WAVE AMPLITUDES AND SPECTRA OBSERVED AT SELECTED BASIN AND RANGE SITES AND IN EASTERN NORTH AMERICA, PHASE 1 FINAL REPORT

VOLUME 1

SEISMIC DATA ANALYSIS CENTER REPORT NO.: SDAC-TR-77-7

AFTAC Project Authorization No.:	VELA T/7709
Project Title:	Seismic Data Analysis Center
ARPA Order No.:	2551
Name of Contractor:	TELEDYNE GEOTECH
Contract No.:	F08606-78-C-0007
Date of Contract:	01 October 1977
Amount of Contract:	$2,674,245
Contract Expiration Date:	30 September 1978
Project Manager:	Robert R. Blandford (703) 836-3882

P. O. Box 334, Alexandria, Virginia 22313

APPROVED FOR PUBLIC RELEASE; DISTRIBUTION UNLIMITED

ABSTRACT

Three Seismic Data Collection System (SDCS) stations were deployed at the Nevada Test Site (NTS) and two in the Eastern United States (EUS) to measure magnitude residuals and spectral differences between NTS and EUS stations. The deployment was intended to determine the degree of anelastic attenuation under NTS. At the Climax Stock (OB2NV) station, the teleseismic body-wave magnitudes are .17 magnitude units (m.u.) lower than at the EUS stations. The magnitudes at the two Pahute Mesa sites are about .2 m.u. higher than at OB2NV, a difference that can be accounted for by amplification of low velocity volcanics under Pahute Mesa. Thus local geology must be taken into account in order to evaluate the attenuation under a given site using amplitude data. This correction shows that with respect to corrected amplitude levels OB2NV is equivalent to Pahute Mesa stations. At all NTS sites the higher frequency content of P waves is significantly less than in the EUS. Available data suggests an attenuation effect of about .2 m.u. under NTS. Measurements at a few other Western United States (WUS) sites, including the site of the SHOAL explosion, yield similar figures. These results confirm that body-waves suffer considerable anelastic losses traversing the mantle under the WUS, including the NTS sites.

TABLE OF CONTENTS

LIST OF FIGURES

LIST OF FIGURES (Continued)

LIST OF FIGURES (Continued)

LIST OF TABLES

INTRODUCTION

Many studies have confirmed the existence of the Western United States (WUS) magnitude anomaly for short-period teleseismic P arrivals that was discovered in the early sixties (Guyton, 1964; Evernden and Clark, 1970; Booth, Marshall and Young, 1974; Der, Massé and Gurski, 1975; North, 1976). The anomaly demonstrates its presence in the form of a regional reduction of teleseismic magnitude measurements at WUS receiving stations compared to those located in the Eastern United States (EUS). A similar anomaly seems to exist for short-period S waves (Der, Massé and Gurski, 1975). In addition, spectral differences exist between short-period body-waves crossing the upper mantle under the WUS and those crossing the mantle under shields or stable platforms (Der and McElfresh, 1977).

Most seismologists attribute the regional magnitude anomaly and spectral differences to anelastic attenuation in the mantle under the WUS. Other types of geophysical anomalies in the WUS, which indicate partial melting in the mantle under the WUS, tend to support this view. This partial melting of

---

Guyton, J. W. (1964). Systematic deviations of magnitude from body-waves at seismograph stations in the United States. Proceedings of VESIAC Conference on Seismic Event Magnitude Determination, University of Michigan, 4410-71-X.

Evernden, J. and D. M. Clark (1970). Study of teleseismic P. II Amplitude data, Phys. Earth. Plant Int., 4, 24-31.

Booth, D. C., P. D. Marshall, and J. B. Young (1974). Long- and short-period amplitudes from earthquakes in the range 0°-114°, Geophys. J. R. Astr. Soc., 39, 523-538.

Der, Z. A., R. P. Massé and J. P. Gurski (1975). Regional attenuation of short-period P and S waves in the United States, Geophys. J. R. Astr. Soc., 40, 85-106.

North, R. G. (1976). Station biases in body-wave magnitude (abstract), Transaction, American Geophysical Union (EOS), 57, 955.

Der, Z. A. and T. W. McElfresh (1977). The relationship between anelastic attenuation and regional amplitude anomalies of short-period P waves in North America, Bull. Seism. Soc. Am., 67, No. 5, 1303-1317.

material, according to experimental and theoretical studies (Walsh, 1968, 1969), must lead to the increase of anelastic attenuation. The spectral differences of P wave arrivals in the WUS versus those of the EUS are such that the size of the magnitude anomaly is roughly consistent with spectral differences, assuming a simple exponential attenuation factor of the form $\exp(-\pi f \Delta t^*)$ where Δt^* is derived from slopes of spectral ratios.

Evoking reciprocity, there is the implication that anelastic attenuation causes a bias in the empirical magnitude-yield relationships based upon NTS data. Therefore, determining the magnitude of the attenuation effect is important.

Previous studies have established the size of the average EUS-WUS regional magnitude bias and spectral differences fairly well ($\Delta m_b \sim .25$, $\Delta t^* \sim .2$). This cannot be said however, for individual receiving stations, because both the Δm_b and Δt^* can differ from the regional value at individual sites. To estimate the amount of anelastic attenuation under individual stations, a detailed study of both Δm_b and Δt^* must be made using many teleseismic events. Because crustal structures can also affect both quantities, efforts must be made to estimate and correct for the crustal effects using the best estimate of the local crustal structure. Such corrections for crustal structure are difficult to make because the structure is not sufficiently known at most places. The properties of near surface layers, which have the most effect on both Δm_b and Δt^*, are especially difficult to estimate. Thus, regional geological information is often not sufficient and local surveys may be necessary.

The authors' past work in simulating the effects of crustal structure indicated that Δm_b may be influenced more by crustal structure than by typical differences in Δt^*. On the other hand formulating a structure that would be able to remove all high frequencies from the spectrum as anelastic attenuation does is difficult if not impossible.

Walsh, J. B. (1968). Attenuation in partially melted material, J. Geophys. Res., 73, 2209-2216.

Walsh, J. B. (1969). New analysis of attenuation in partially melted rock, J. Geophys. Res., 74, 4333-4337.

To investigate the question of the existence of high anelastic attenuation under NTS, three Special Data Collection System (SDCS) seismic stations were deployed to that area. One station, OB2NV, was placed on Climax Stock, a Cretaceous granitic intrusive body, the site of the HARDHAT and PILE-DRIVER nuclear explosions. Two other stations, NTNV and NT2NV, were placed on the Pahute Mesa, a deep volcanic caldera (Silent Canyon Volcanic Crater), which is filled with low velocity [α ~ 3.6 km/sec average] Tertiary volcanic tuffs and rhyolites to a depth of at least 4 km. Spence (1974) predicted, based upon gravity data, a thickness of about 5 km. Two other SDCS stations remained at their previous locations: Red Lake, Ontario (RKON) and Houlton, Maine (HNME). A key station at NTS is OB2NV which, like RKON, is located on granite, the test medium of greatest interest. HNME is located in a region where there are indications of some attenuation in the upper mantle (Solomon and Toksöz, 1970; Der, Masse and Gurski, 1975). NT2NV and NTNV are less diagnostic because they are located above the thick low-velocity caldera fill and (possibly) a deep, buried volcanic plug which was hypothesized by Spence (1974). The locations of the stations used in this study are shown in Figure 1. In this figure we also show the LRSM stations SZNV, SEMN, CUNZ, and EKNV also analyzed in this report.

Spence, W. (1974). P wave residual differences and inferences on an upper mantle source for the Silent Canyon Volcanic Centre, Southern Great Basin, Nevada, Geophys. J. R. Astr. Soc., 38, 505-523.

Solomon, S. C. and M. N. Toksöz (1970). Lateral variation of attenuation of P and S waves beneath the United States, Bull. Seism. Soc. Am., 60, 819-838.

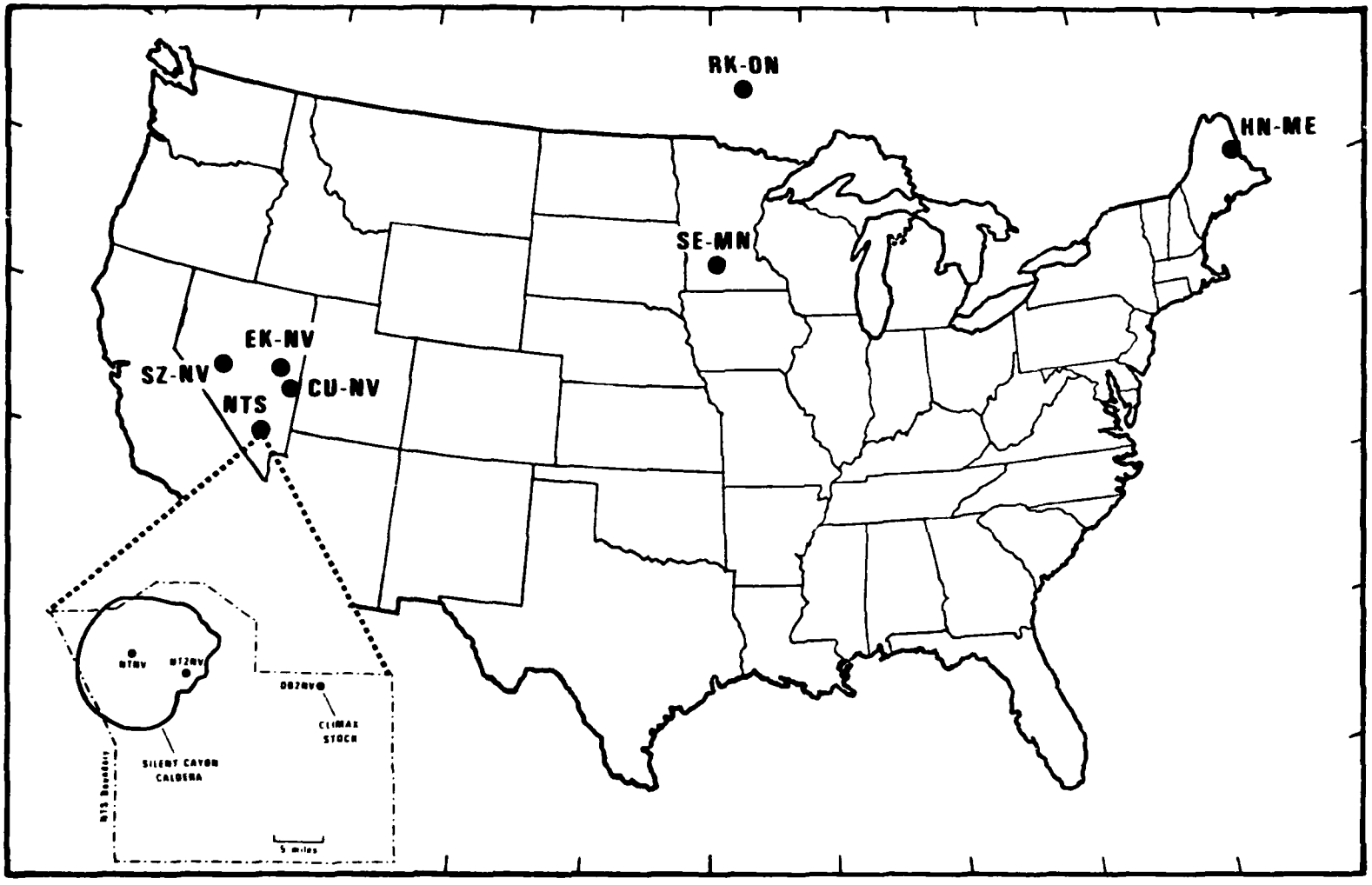

Figure 1. Map of station locations used in this study

DATA ANALYSIS

Body-Wave Magnitudes

Short-period data at the SDCS sites were recorded on digital tape at 20 samples/second. Amplitudes, dominant periods and arrival times were read for each available station using the CRT display of traces on the PDP-15 computer for a set of 119 events that covered the period between 1 September 1976 to 31 March 1977.

Events used, along with the amplitude and period readings and magnitudes computed at each station, are given in Appendix A. Magnitudes are also given in the table for each event, when available. Magnitudes (m_b) were computed with the formula

$$m_b = \log_{10}(\frac{A}{T}) + B(\Delta) \qquad (1)$$

where A is the amplitude in millimicrons (mμ) (corrected for instrument amplification at the measured period) and T is the dominant period of the signal. $B(\Delta)$ are Gutenberg and Richter's (1956) (peak-to-peak) distance correction factors for zero hypocentral depth. We also computed "magnitudes" without dividing by the period, but correcting the amplitudes for instrument response at the measured period. We shall call these values "uncorrected" in this report.

$$m_b^{(\text{uncorrected})} = \log_{10}(A_{m\mu}) + B(\Delta) \qquad (2)$$

The "uncorrected" magnitudes minimize the magnitude effect due to attenuation. As the signal decreases in amplitude due to attenuation, the lower frequencies are less affected and the dominant period increases. The system magnification is less at long periods so that the amplitude corrected for instrument response at the larger value of T tends to remain constant. Dividing by T tends to again reduce the magnitude. Thus when T is not divided out, the magnitude tends to remain the same as attenuation increases. The greatest difference in amplitude is seen on the raw traces, uncorrected for instrument response. These differences are not given in this report.

Results of this study are displayed in a set of histograms showing magnitude differentials, dominant periods and Δt^* between all possible pairs

---

Gutenberg, B. and C. F. Richter 1956, Magnitude and energy of earthquakes, Ann. Geof. (Rome), 9, 1-15.

of individual stations. In each histogram we calculated the standard deviation (σ), the mean value, and its approximate 95% confidence limits $\pm 2\sigma_{mean}$ where $\sigma_{mean} = \sigma/\sqrt{N}$ (assuming normality). For small samples ($n < 30$) we give confidence limits based on the "Student's t" distribution (Hoel, 1954). We also print the total number of data points used on each histogram. We did not use any readings at epicentral distances greater than 85°. This was done to eliminate the effect of apparent low Q due to diffraction close to the core-mantle boundary.

Figures 2 through 29 show histograms for magnitude differentials, both corrected and uncorrected, as well as differences in dominant P wave periods for all possible station pairs. Period histograms for HNME were not included because a different instrument response at this station made any comparison invalid.

Figure 2, which shows the RKON-OB2NV pair, is the most diagnostic discussed here. The corrected magnitudes are significantly less at OB2NV than at RKON. Despite the large number of data points (76) used, the confidence limits are still quite wide (±.114). Although the sign of the mean is still positive, which may indicate lower amplitudes at OB2NV, the "uncorrected" magnitude differentials (Figure 3) do not show a significant bias. While this situation does not rule out the existence of an uncorrected magnitude (amplitude) differential, it does show that the differential can be anywhere between -.04 to .21 (95% limits). Since about seven months of data are shown, and the scatter yields 95% confidence limits of $\pm$.1, the sites should be occupied for about two years with the same average rate of data acquisition, quadrupling the data to narrow the confidence limits to about ±.05 magnitude units. The difference in average P wave periods (Figure 4) is also significant which, since the dominant periods at this station are longer, supports the hypothesis of higher attenuation under OB2NV. (Average P wave period at RKON is .70 seconds vs 0.88.)

In contrast, when NT2NV and NTNV are compared, no significant difference is found between the two stations either in magnitude or dominant period

---

Hoel, P. G. 1954, Introduction to Mathematical Statistics: New York, John Wiley & Sons.

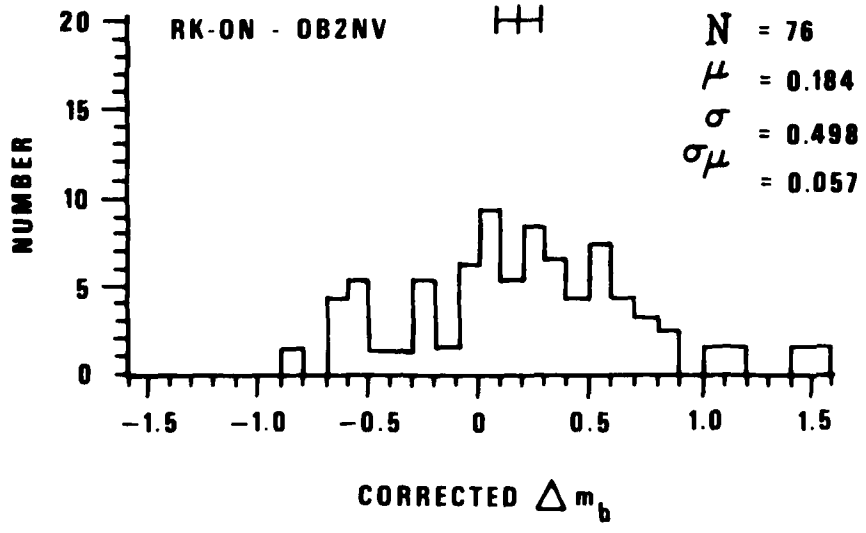

Figure 2. Histogram of magnitude differentials RKON-OB2NV

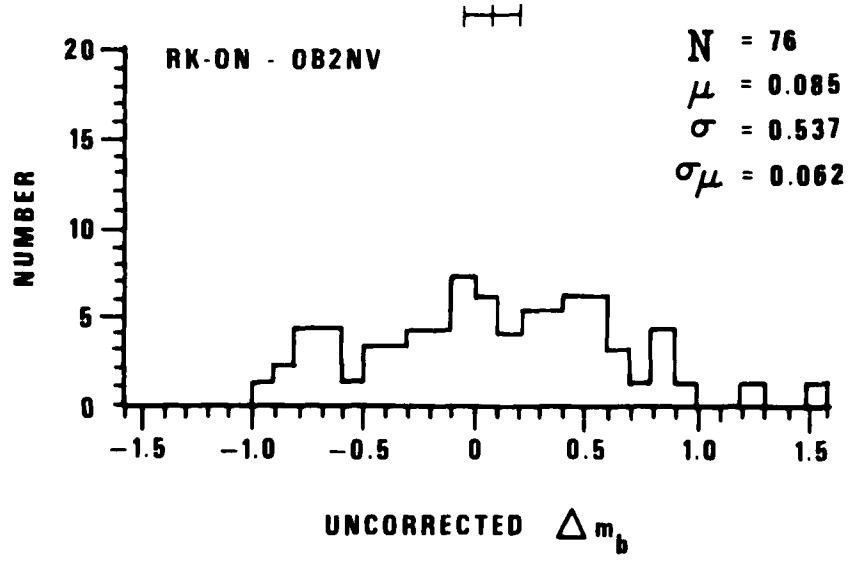

Figure 3. Histogram of uncorrected magnitude differentials RKON-OB2NV

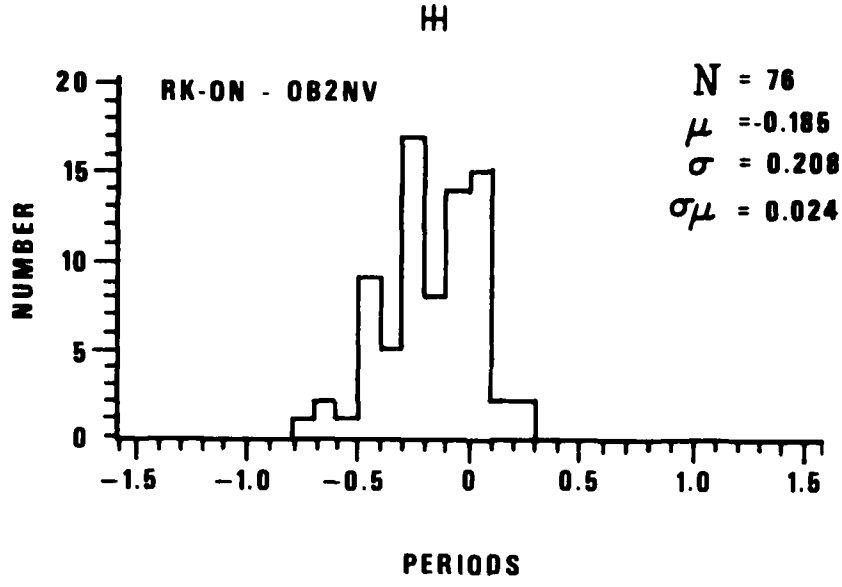

Figure 4. Histogram of differences in dominant P wave periods RKON-OB2NV

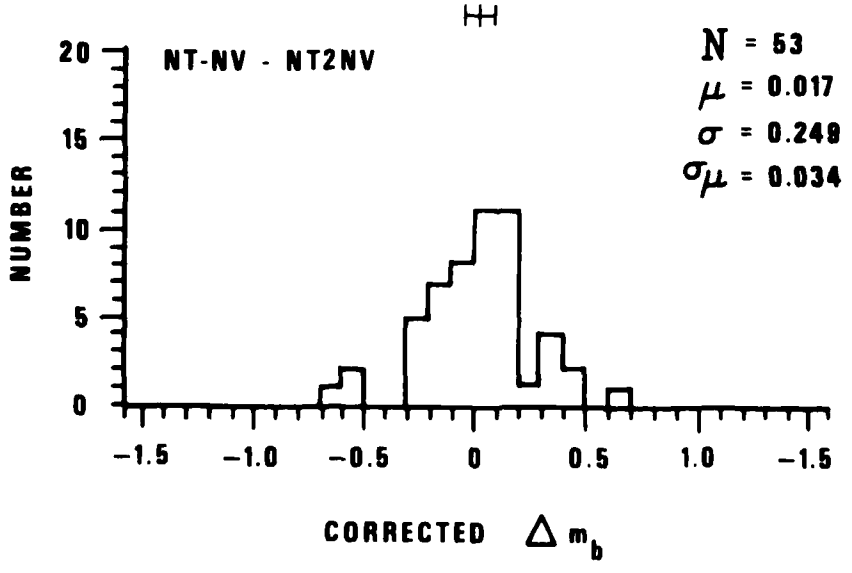

Figure 5. Histogram of magnitude differentials NTNV-NT2NV

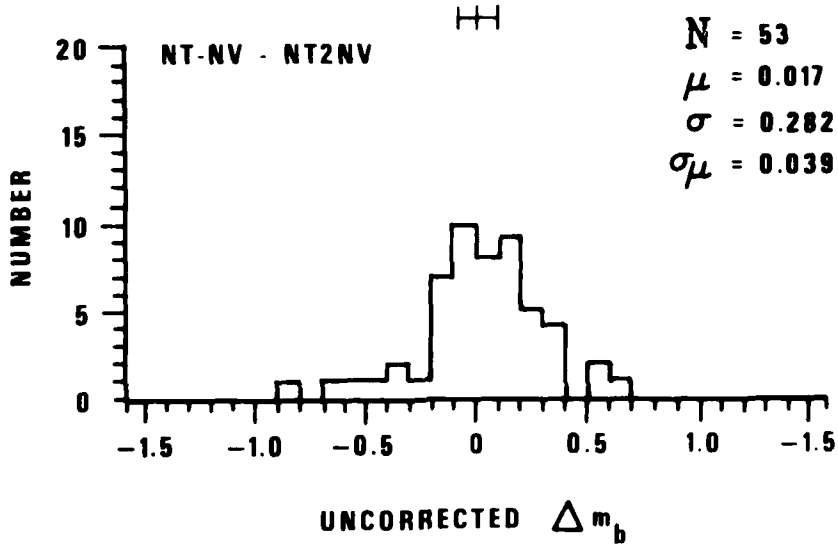

Figure 6. Histogram of uncorrected magnitude differentials NTNV-NT2NV

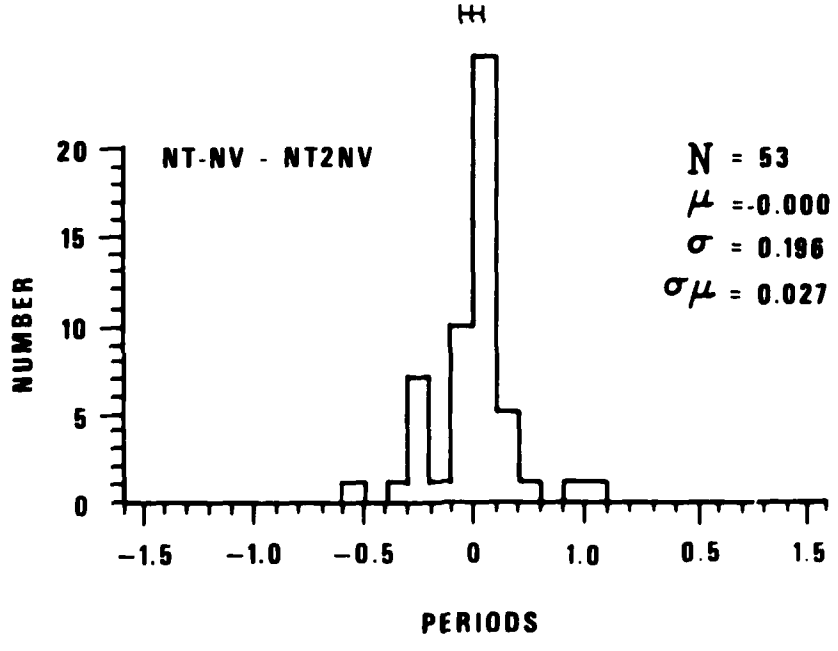

Figure 7. Histogram of differences in dominant P wave periods NTNV-NT2NV

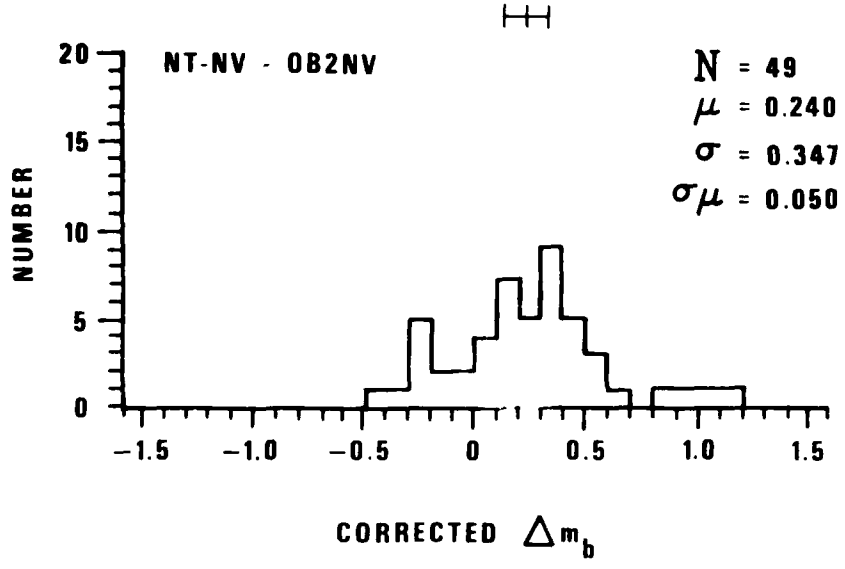

Figure 8. Histogram of magnitude differentials MTNV-OB2NV

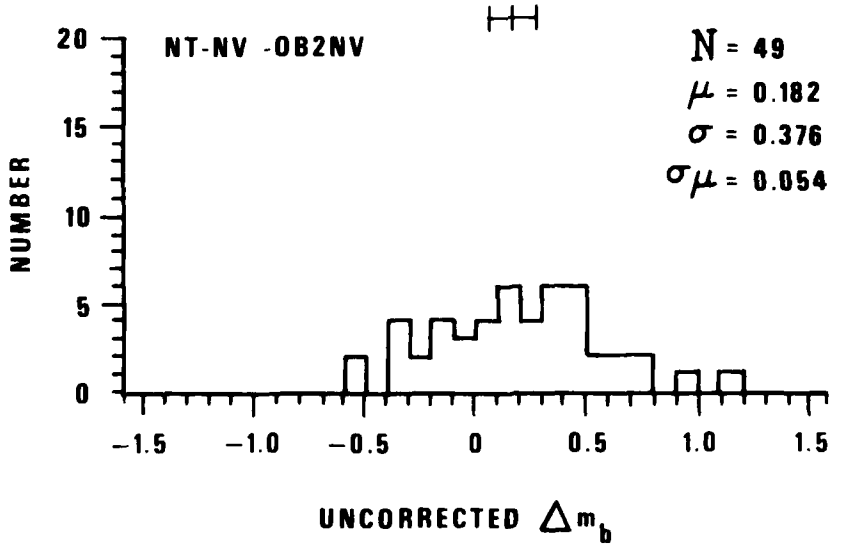

Figure 9. Histogram of uncorrected magnitude differentials MTNV-OB2NV

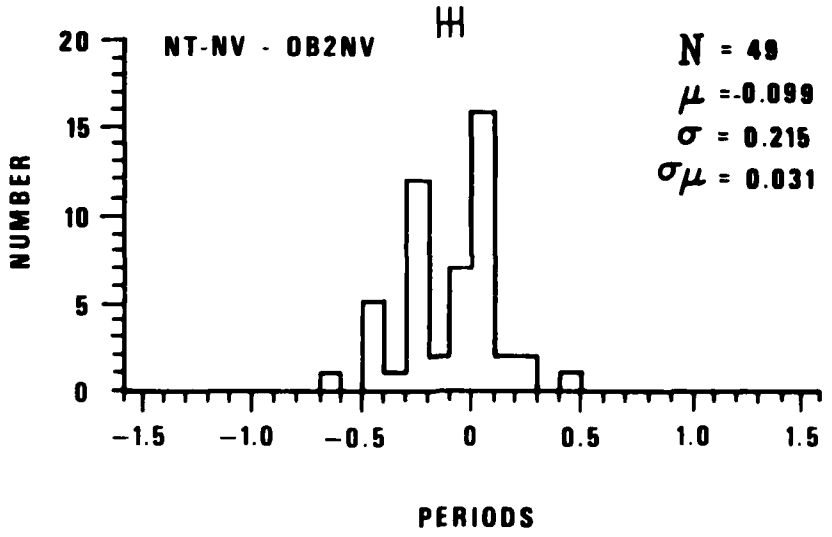

Figure 10. Histogram of differences in dominant P wave periods NTNV-OB2NV

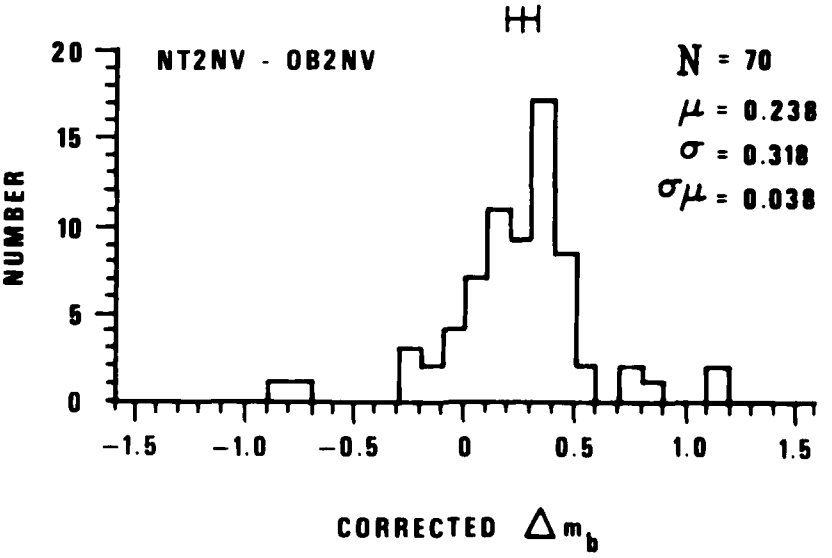

Figure 11. Histogram of magnitude differentials NT2NV-OB2NV

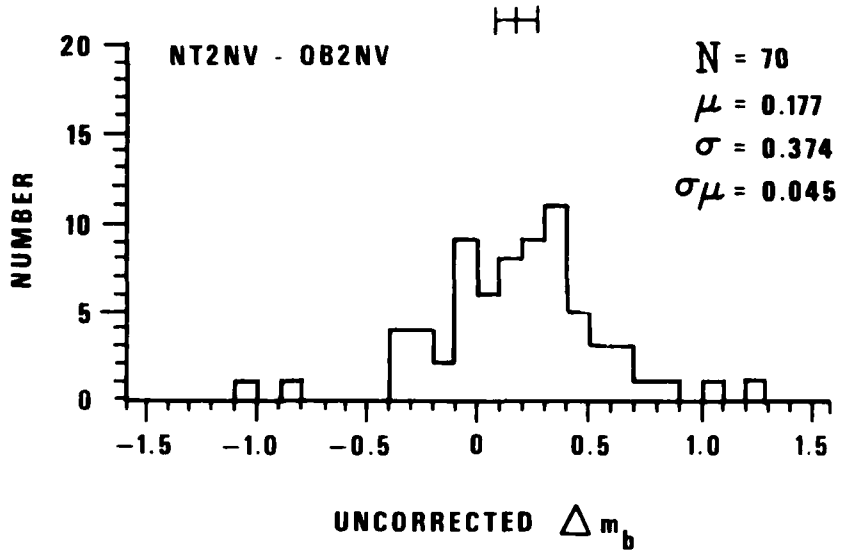

Figure 12. Histogram of uncorrected magnitude differentials NT2NV-OB2NV

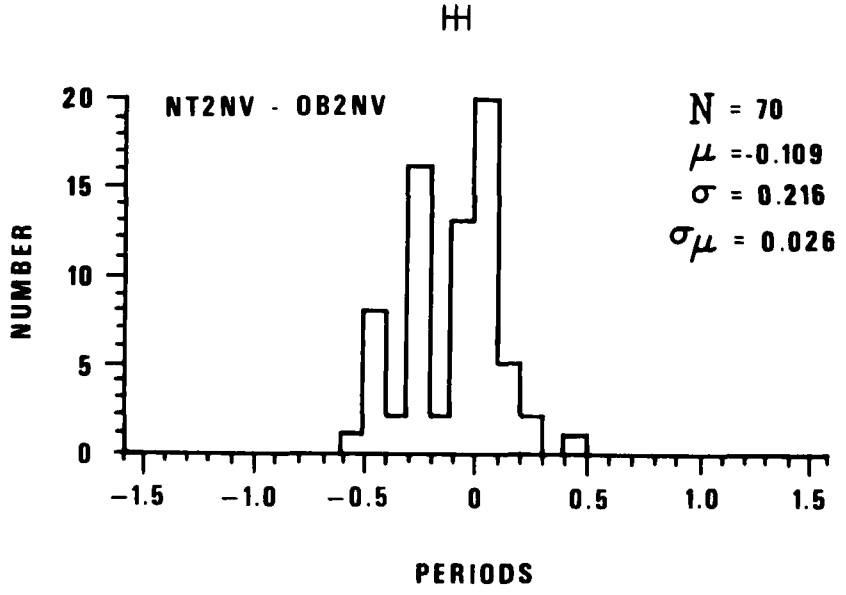

Figure 13. Histogram of differences in dominant P wave periods NT2NV-OB2NV

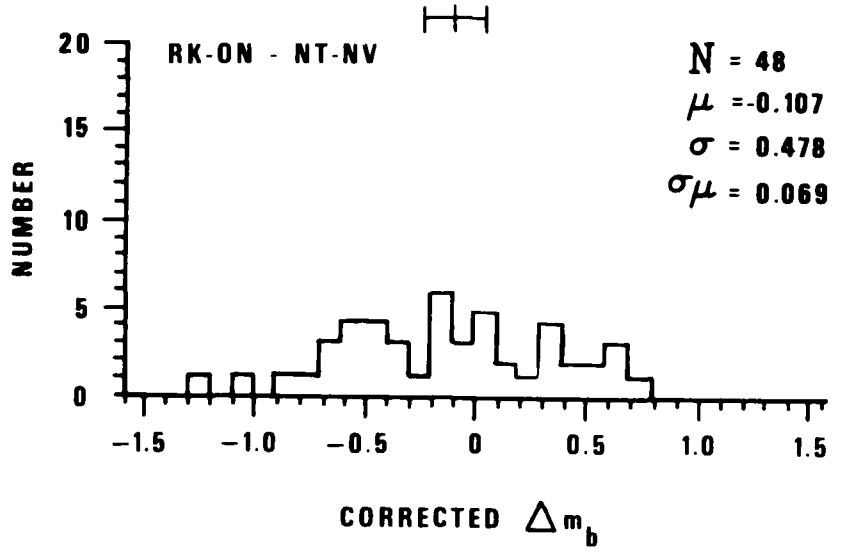

Figure 14. Histogram of magnitude differentials RKON-NTNV

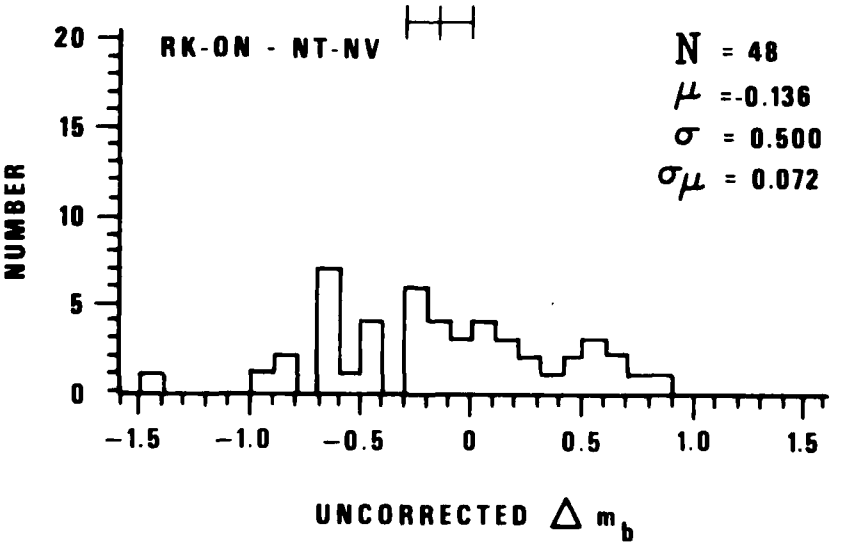

Figure 15. Histogram of uncorrected magnitude differentials RKON-NTNV

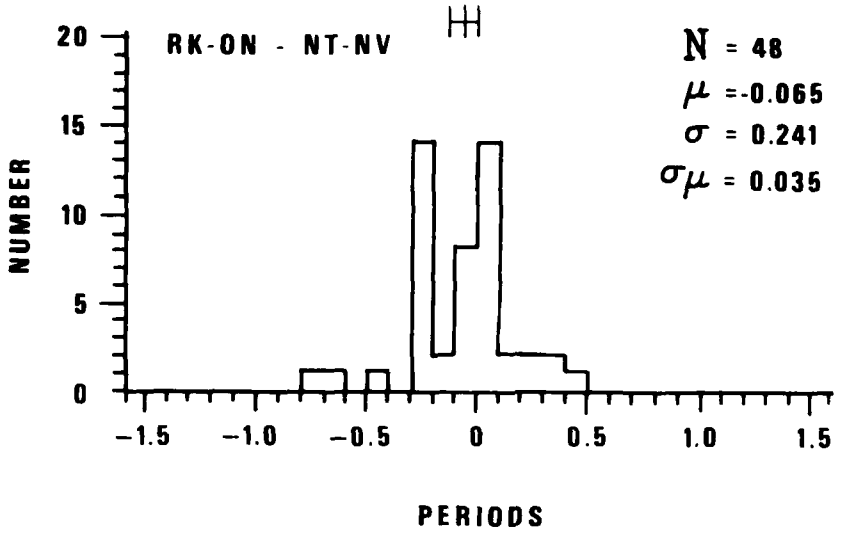

Figure 16. Histogram of differences in dominant P wave periods RKON-NTNV

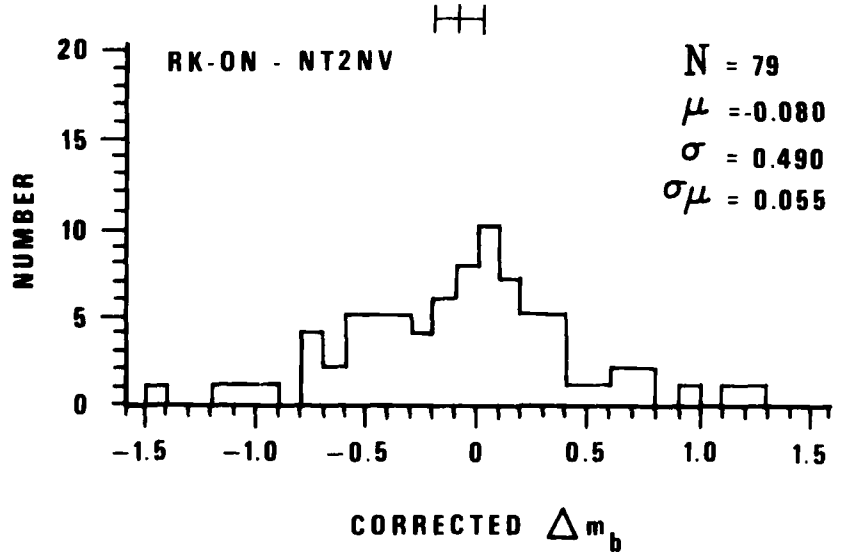

Figure 17. Histogram of magnitude differentials RKON-NT2NV

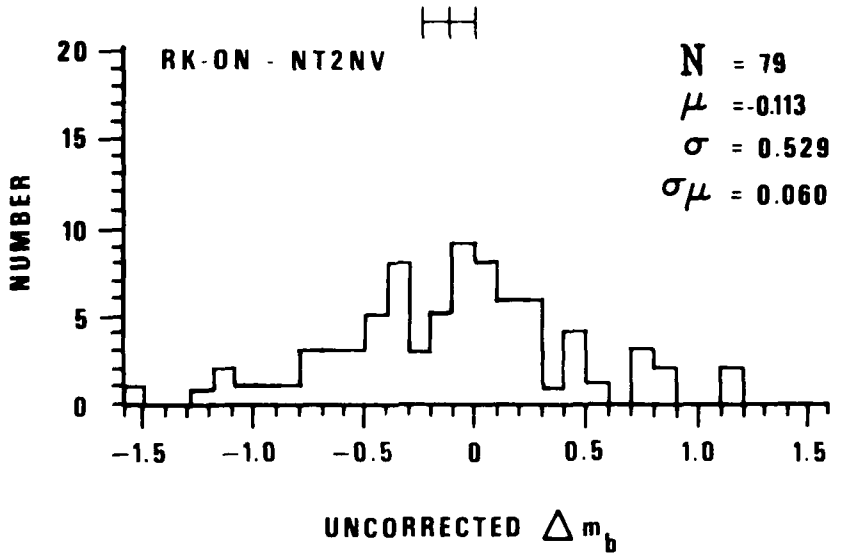

Figure 18. Histogram of uncorrected magnitude differentials RKON-NT2NV

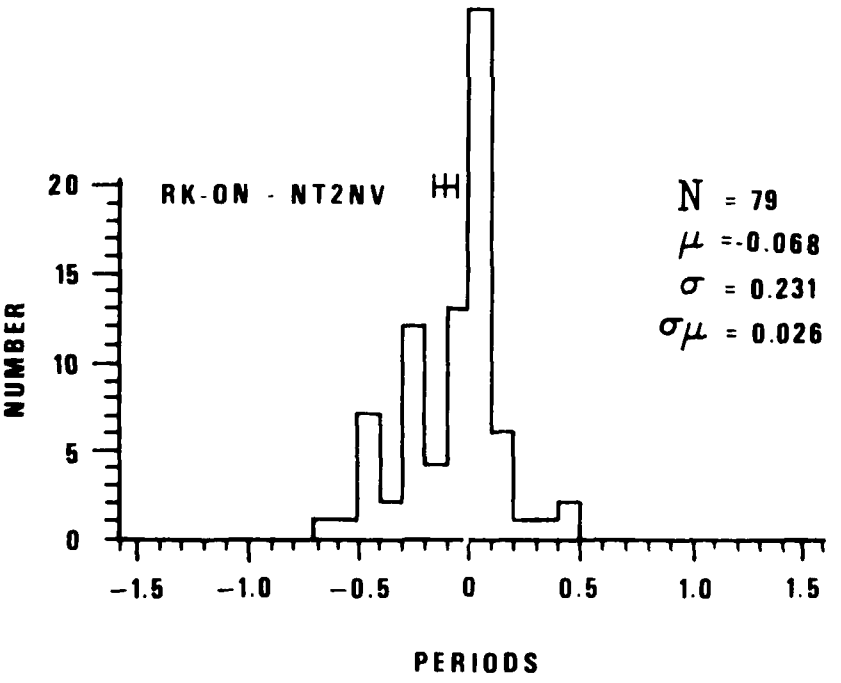

Figure 19. Histogram of differences in dominant P wave periods RKON-NT2NV

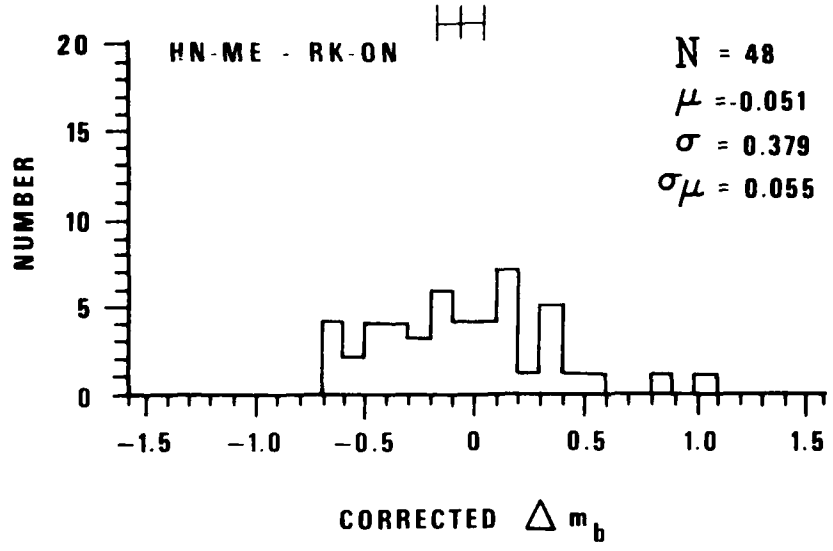

Figure 20. Histogram of magnitude differentials HNME-RKON

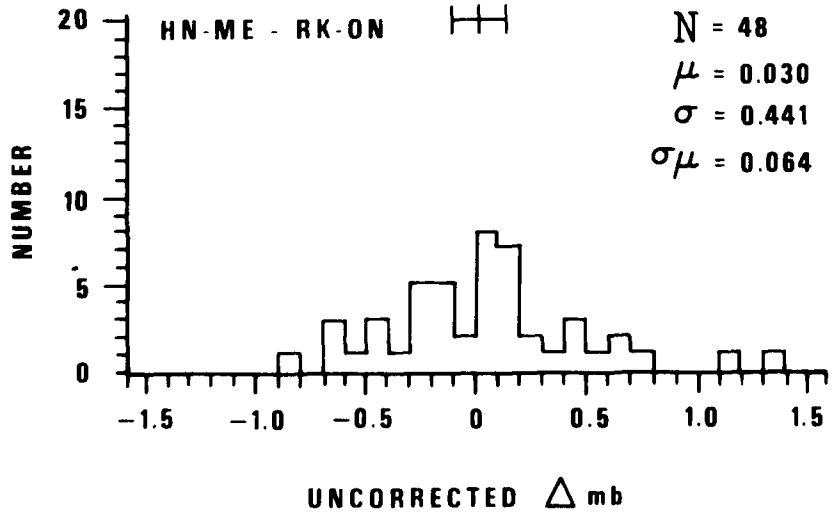

Figure 21. Histogram of uncorrected magnitude differentials HNME-RKON

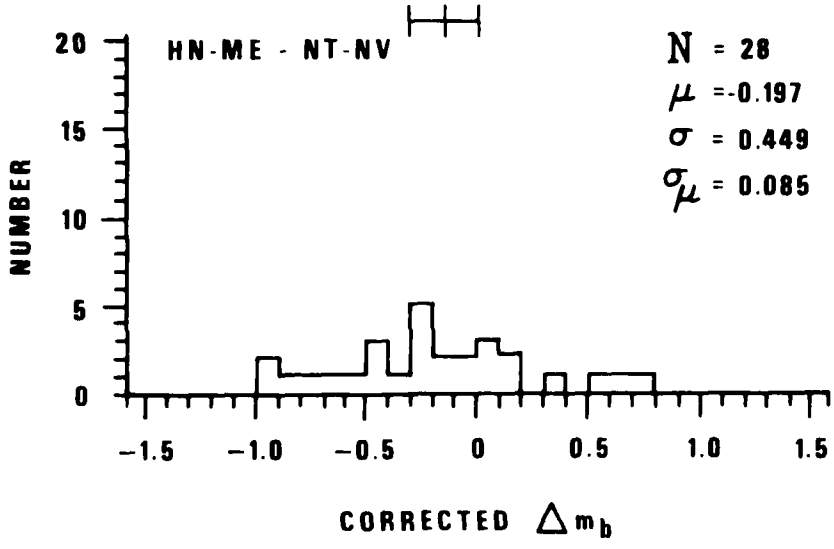

Figure 22. Histogram of magnitude differentials HNME-NTNV

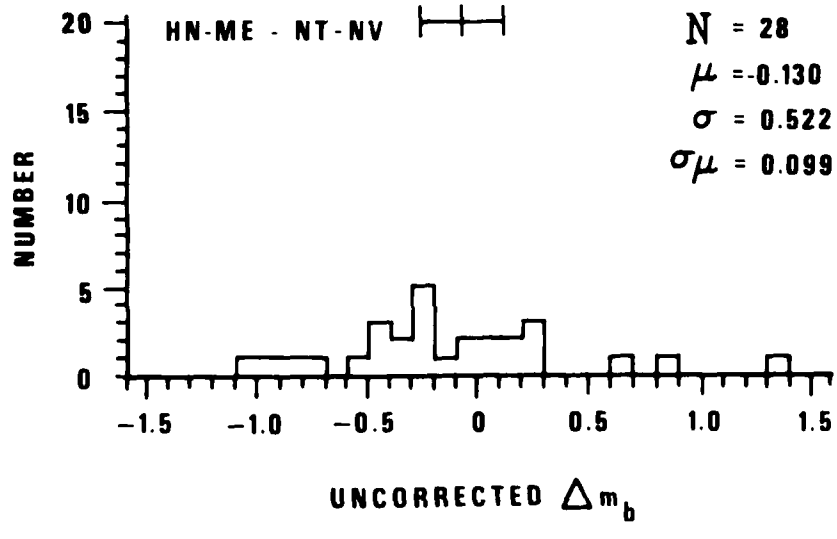

Figure 23. Histogram of uncorrected magnitude differentials HNME-NTNV

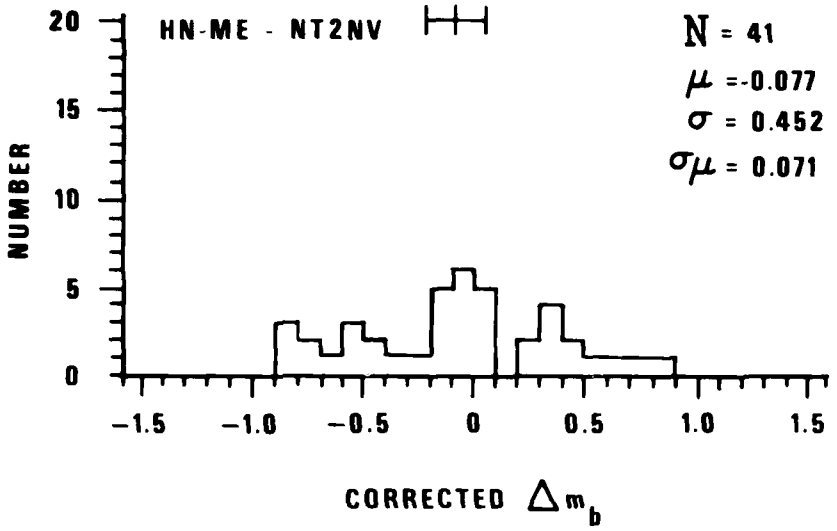

Figure 24. Histogram of magnitude differentials HNME-NT2NV

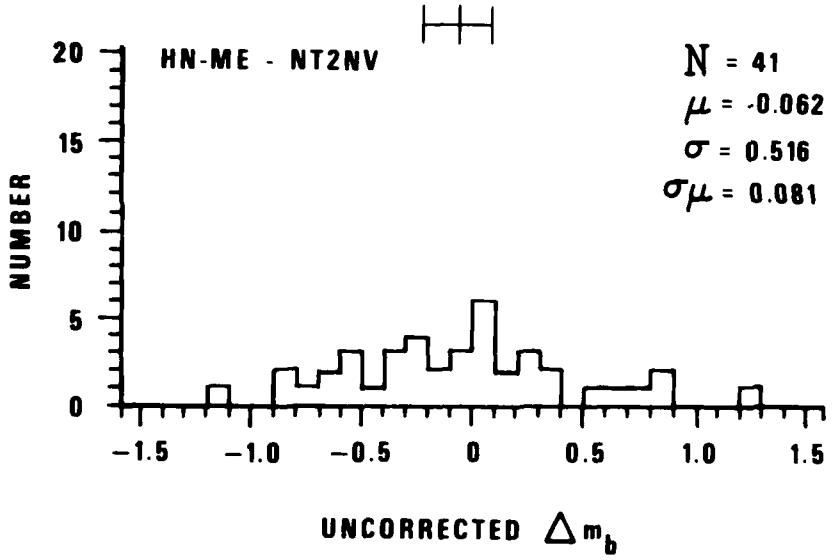

Figure 25. Histogram of uncorrected magnitude differentials HNME-NT2NV

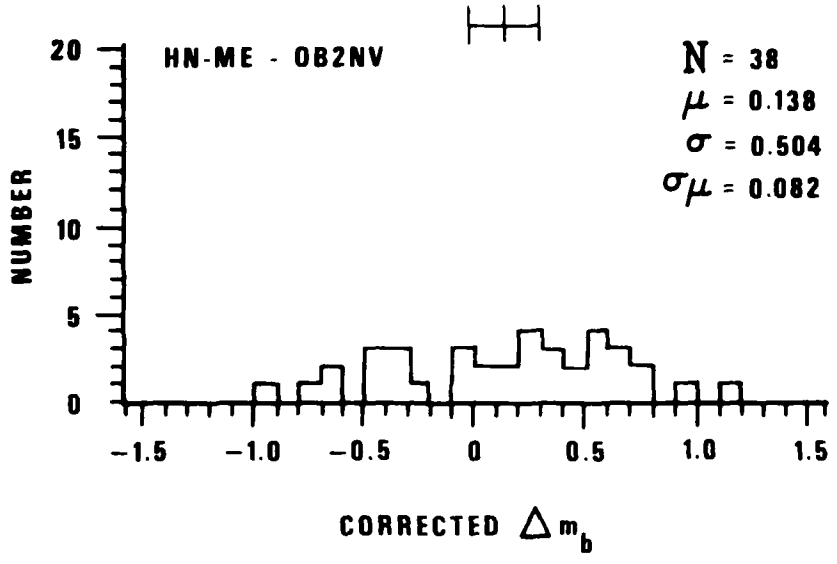

Figure 26. Histogram of magnitude differentials HNME-OB2NV

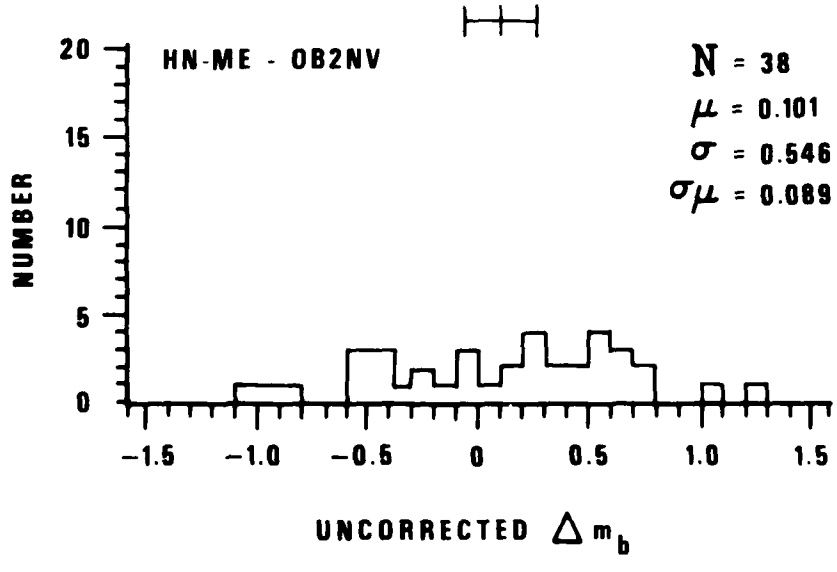

Figure 27 Histogram of uncorrected magnitude differentials HNME-OB2NV.

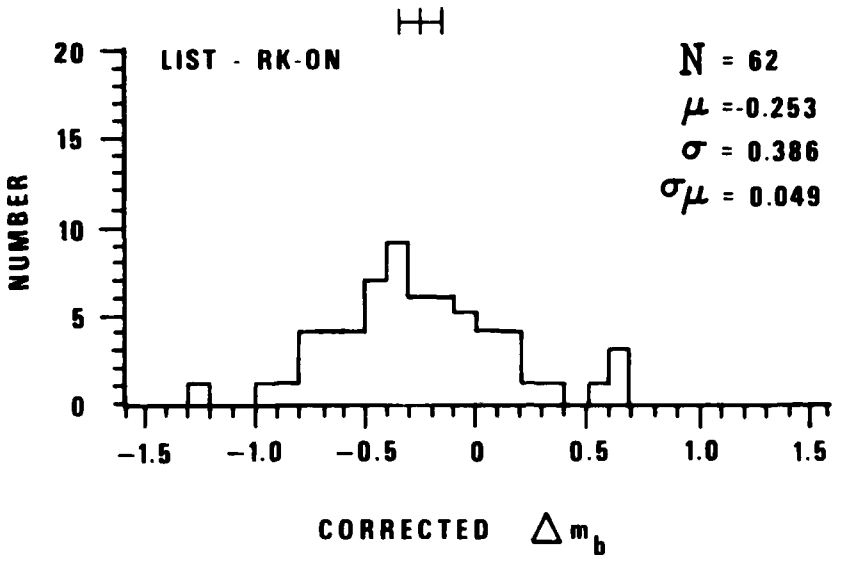

Figure 28. Histogram of List-RKON magnitude differentials

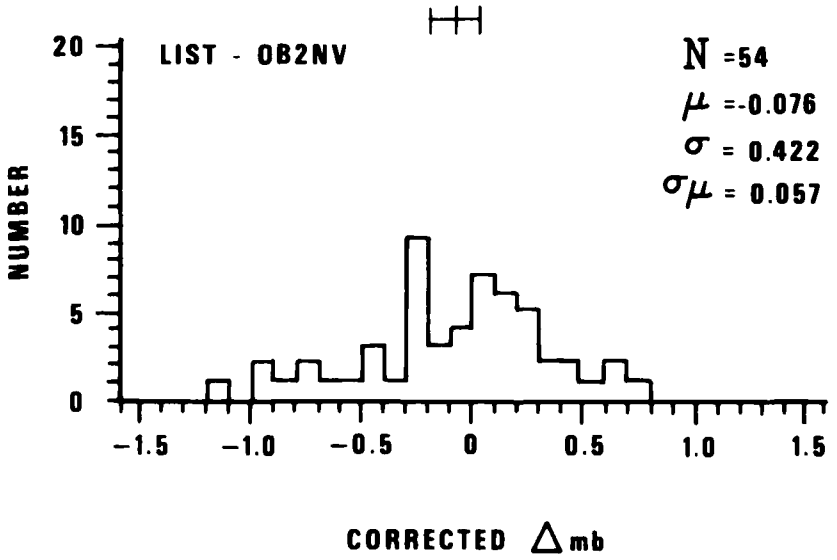

Figure 29. Histogram of List-OB2NV magnitude differentials

(Figures 5 through 7).

Considerable difference exists, however, between OB2NV and the two Pahute Mesa stations (Figures 8 through 13). Amplitudes are considerably higher and the dominant periods shorter at Pahute Mesa than on the Climax Stock.

Magnitudes, and amplitudes, at Pahute and RKON are roughly on the same level and the dominant periods are intermediate between RKON and OB2NV (Figures 14 through 19). Calculations in the subsequent sections of this report shows that because of the low-velocity crustal layers, amplitudes at Pahute are 0.2 log amplitude higher than they would be on granite, a result that brings the RKON-NT2NV and RKON-NTNV amplitude differences into rough agreement with the RKON-OB2NV differences.

Note that the mean of standard deviations of Δm_b measurements at the three NTS sites, compared to RKON, is almost twice the mean standard deviation of the relative Δm_b among pairs of NTS stations. This situation is at least partially a result of the events' radiation patterns, which cause a greater variability between azimuths to the RKON-NTS station pairs from the epicenters, while the NTS stations are set at almost the same point in the radiation patterns, suggesting an alternative way to determine RKON to NTS bias using a reference station, denoted by X, close to NTS that, together with RKON, has been operational for a long time. Thus, the bias of station X, relative to RKON, could, using a large number of events, be measured with great precision. From this point deducing the station X-NTS bias (and RKON-NTS) using fewer events since this pair would be less affected by radiation patterns would be a simple matter. The proximity of station X to NTS could also be useful in measuring identical portions of the wavetrain, which has been done for the SZNV-MNNV station pair in the past (Der and McElfresh, 1975). The SRO station ANMO may also be used this way because North (1976) determined its magnitude bias with great precision.

Der, Z. A. and T. W. McElfresh (1975). Short-period P wave attenuation along various paths in North America as determined from P wave spectra of the SALMON nuclear explosion, SDAC-TR-75-16, Teledyne Geotech, Alexandria, Virginia 22314.

North, R. G. (1976). Station biases in body-wave magnitude (abstract), Transactions, American Geophysical Union (EOS), 57, 955.

Located in an area of high microseismic noise and suspected higher attenuation, HNME, the last station discussed here, is the least valuable for our study (Solomon and Toksöz, 1970; Der, Massé and Gurski, 1975). Because of the high noise level there were considerably fewer readings at this station, but no significant bias was found relative to RKON (Figures 20 and 21). Comparisons of dominant periods involving HNME readings are not shown because instrument response at this station was significantly less peaked at high frequencies than at other stations used in this study. The magnitude comparisons are valid, however, since instrument response is corrected. Comparison of HNME magnitudes with the NTS stations are inconclusive due to wide confidence limits (Figures 22 through 27).

Comparison of magnitudes in the list with our data show that those magnitudes agree with readings at OR2NV and are, consequently, significantly lower than RKON magnitudes (Figures 28 and 29).

Table I summarizes the results of the magnitude study at SDCS stations.

Spectral Ratio Studies

In addition to magnitude measurements relative t* values were also computed for all combinations of station pairs for a set of selected events. The Δt^* estimates were obtained by fitting a straight line to the logarithm of the amplitude spectral ratio between each pair of stations. The signal window was of 12 sec duration. This procedure is identical to that described in a previous report (Der and McElfresh, 1976b), but for completeness it is summarized in the next section. A 3-second signal window was also used for many of the events because we suspected that the early part of the signal might be more diagnostic. However, the basic features of most spectra computed from 3-second signal windows remained the same as those from 12-second windows, although the variance of Δt^* increased. (In this report only the Δt^* computed from 12-second windows are used.) The individual Δt^* determinations are tabulated in Table II.

Der, Z. A. and T. W. McElfresh (1976b). The effect of attenuation on the spectra of P waves from nuclear explosions in North America, SDAC-TR-76-7, Teledyne Geotech, Alexandria, Virginia 22314.

TABLE I

Summary of SDCS Magnitude Study

STATION PAIR	CORRECTED m_b		UNCORRECTED m_b		PERIODS	
	μ	$2\sigma_\mu$	μ	$2\sigma_\mu$	μ	$2\sigma_\mu$
RKON-OB2NV	0.184	0.114	0.085	0.123	-0.185	0.048
NTNV-NT2NV	0.017	0.068	0.017	0.077	0.000	0.054
NTNV-OB2NV	0.240	0.099	0.182	0.107	-0.099	0.061
NT2NV-OB2NV	0.238	0.076	0.177	0.089	-0.109	0.052
RKON-NTNV	-0.107	0.138	-0.136	0.144	-0.065	0.070
RKON-NT2NV	-0.080	0.110	-0.113	0.119	-0.068	0.052
HNME-RKON	-0.051	0.109	0.030	0.127		
HNME-NTNV	-0.197	0.177	-0.130	0.206		
HNME-NT2NV	-0.077	0.141	-0.062	0.161		
HNME-OB2NV	0.138	0.163	0.101	0.177		
LST-RKON	-0.253	0.098				
LST-OB2NV	-0.076	0.115				

TABLE II

Results of all Δt* measurements between SDCS station pairs

NT2/HN	NT2/RK	NT2/OB2	NT2/NT	NT/HN	NT/RK	NT/OB2	OB2/HN	OB2/RK	RK/HN					
******	0.030	-0.060	0.020	******	-0.020	-0.100	******	0.200	******	30	SEP	76	8	4	10.	0
-0.030	-0.180	-0.370	-0.130	0.150	-0.040	-0.130	0.300	0.190	0.110	22	SEP	76	8	16	9.	3
******	******	-0.160	-0.080	******	******	-0.050	******	******	******	22	SEP	76	8	26	27.	6
******	0.510	-0.510	******	******	******	******	******	0.270	******	22	SEP	76	2	30	30.	8
-0.100	0.190	-0.270	-0.004	-0.380	0.180	-0.080	-0.010	0.260	-0.240	29	SEP	76	3	0	0.	0
-0.010	0.010	-0.120	0.110	-0.180	0.700	-0.070	-0.130	0.740	-0.290	4	OCT	76	23	36	6.	0
******	******	******	******	******	******	******	******	******	-0.220	23	NOV	76	5	3	0.	0
******	******	******	******	******	******	******	******	0.260	******	10	OCT	76	2	58	56.	6
******	******	******	******	******	******	******	******	0.080	******	9	OCT	76	21	10	24.	1
-0.110	0.050	-0.020	******	******	******	******	0.0	0.200	0.010	9	OCT	76	16	2	26.	9
******	******	******	******	******	******	******	******	0.180	******	12	OCT	76	23	49	24.	3
******	0.130	-0.030	0.010	******	0.110	-0.070	******	0.170	******	22	OCT	76	4	4	22.	6
******	-0.020	-0.190	-0.050	******	-0.010	-0.170	******	0.150	******	22	OCT	76	5	53	50.	9
******	-0.220	0.120	******	******	******	******	******	0.230	******	22	OCT	76	18	35	23.	9
0.220	0.170	0.004	0.020	0.190	0.170	-0.020	0.220	0.260	-0.030	9	OCT	76	12	31	6.	6
0.040	-0.100	-0.080	-0.100	0.110	0.0	-0.020	0.100	-0.0	0.100	26	OCT	76	1	50	56.	4
******	******	******	******	******	******	******	******	-0.660	******	13	OCT	76	17	35	45.	1
0.030	******	0.160	******	******	******	******	0.240	******	******	2	NOV	76	19	23	2.	7
******	******	******	******	******	0.090	******	******	******	******	23	NOV	76	20	0	2.	7
******	0.270	******	******	******	******	******	******	******	******	3	DEC	76	2	27	34.	4
******	0.040	******	******	******	******	******	******	******	******	3	DEC	76	23	10	23.	1
-0.410	-0.260	******	******	******	******	******	******	******	-0.210	30	NOV	76	0	40	37.	1
-0.240	-0.130	******	******	******	******	******	******	******	-0.360	1	DEC	76	14	15	33.	2
******	0.730	******	-0.060	******	0.690	******	******	******	******	26	NOV	76	23	43	12.	6
******	0.280	******	-0.010	******	0.270	******	******	******	******	4	DEC	76	12	32	35.	4
******	******	0.290	-0.070	******	******	0.140	******	******	******	5	JAN	77	22	44	57.	0
******	-0.080	******	******	******	******	******	******	******	******	13	DEC	76	23	1	28.	0
******	-0.140	******	******	******	******	******	******	******	******	1	DEC	76	17	48	53.	0
******	******	******	******	-0.030	-0.110	******	******	******	0.050	29	DEC	76	10	18	58.	0
******	0.130	******	******	******	******	******	******	******	******	20	DEC	76	21	22	55.	0
******	-0.060	-0.510	-0.030	******	0.110	-0.510	******	0.600	******	6	JAN	77	7	55	55.	0
******	******	******	******	******	******	******	******	0.310	******	27	DEC	76	18	8	8.	0
******	0.270	******	0.080	******	0.200	******	******	******	******	7	DEC	76	0	36	44.	0
******	******	-0.010	0.020	******	******	-0.020	******	******	******	1	JAN	77	11	33	42.	0
******	-0.030	-0.150	******	******	******	******	******	0.120	******	31	DEC	76	0	16	37.	0
******	******	0.020	0.130	******	******	-0.020	******	******	******	5	JAN	77	10	37	33.	6
******	0.520	0.150	0.280	******	0.140	-0.170	******	0.370	******	6	JAN	77	16	2	3.	6
******	******	0.0	0.150	******	******	-0.060	******	******	******	17	JAN	77	6	23	42.	5
******	0.120	-0.170	-0.070	******	0.210	-0.110	******	0.120	******	17	JAN	77	0	42	22.	5
******	0.260	******	******	******	******	******	******	******	******	4	DEC	76	5	6	26.	7
******	-0.270	-0.400	******	******	******	******	******	0.200	******	24	JAN	77	6	11	30.	0
******	******	******	******	******	******	******	******	0.350	******	29	JAN	77	4	24	25.	0
******	0.460	-0.040	******	******	******	******	******	0.250	******	3	FEB	77	21	30	50.	0
0.040	0.080	-0.170	******	******	******	******	******	0.260	******	6	FEB	77	0	31	29.	0
******	-0.090	-0.100	******	******	******	******	******	0.200	-0.050	13	FEB	77	5	51	11.	0
******	0.100	******	******	******	******	******	******	0.0	******	17	FEB	77	13	32	7.	0
******	0.060	******	******	******	******	******	******	******	******	16	FEB	77	6	56	18.	0
******	0.110	-0.010	******	******	******	******	******	0.110	******	16	FEB	77	1	6	48.	0
******	0.080	-0.080	******	******	******	******	******	0.130	******	19	FEB	77	20	51	26.	0
******	0.010	-0.040	******	******	******	******	******	0.060	******	19	FEB	77	5	51	1.	0
******	-0.170	-0.190	******	******	******	******	******	-0.030	******	19	FEB	77	22	33	55.	0
******	-0.140	-0.150	-0.170	******	0.240	-0.020	******	0.290	******	25	FEB	77	8	7	36.	0
******	-0.180	0.160	******	******	******	******	******	-0.080	******	7	MAR	77	0	11	55.	0
******	0.510	0.060	0.220	******	0.260	-0.230	******	0.500	******	8	MAR	77	22	46	44.	0
******	0.130	0.050	0.040	******	0.030	******	******	0.190	******	12	MAR	77	2	58	55.	0
******	-0.060	-0.060	0.130	******	-0.220	-0.250	******	0.360	******	13	MAR	77	4	55	55.	0
******	-0.130	-0.140	-0.250	******	0.130	-0.290	******	0.110	******	15	MAR	77	21	28	9.	0
******	******	-0.090	-0.250	******	******	-0.230	******	******	******	19	MAR	77	10	56	6.	0
******	******	-0.100	-0.050	******	******	-0.050	******	******	******	21	MAR	77	4	36	38.	0
******	0.060	0.050	0.020	******	0.100	0.090	******	-0.010	******	23	MAR	77	2	11	45.	0
										26	MAR	77	4	36	10.	0

Figures B1 to B20 in the Appendix display the signal traces for events studied. An "X" marks traces omitted from the compilation of spectral results because of poor S/N ratio. An asterisk (*) marks traces excluded because the hypo-central distance exceeded 85°. Figures C1 to C80 show all spectra computed and Figures D1 to D80 show all amplitude spectral ratios with straight-line fits.

The resulting mean Δt^* values, as well as the standard deviation, standard deviation of the mean, and the 95% confidence limits on the mean are displayed as histograms. Positive values of Δt^* indicate that the station spectrum in the denominator is richer in high frequencies. The general trend emerging from these histograms is similar to the trend derived from magnitude and period data. OB2NV is again distinguished by the low-frequency character of its P wave arrival when compared to RKON (Figure 30). The mean Δt^* is about 0.196, which can explain a 0.23 magnitude bias at 1 Hz. The difference between NT2NV and NTNV is small and not significant (Figure 31), but both stations are richer in high frequencies than OB2NV (Figures 32 and 33). Both Pahute Mesa stations are, in turn, significantly lower in high frequency content of P waves than RKON (Figures 34 and 35), indicating their intermediate position between OB2NV and RKON. No conclusions can be made at the 95% confidence level from the histograms involving HNME because of the small number of available ratios (Figures 36 through 39).

In summary, the spectral analyses provide a picture that is qualitatively consistent with magnitude biases and visual observations of dominant periods. The most important results of the Δt^* study are shown in Table III.

Note that the observed differences in dominant periods of P waves in the EUS and WUS, respectively, are of the order of .1-.2 sec (the average period for teleseismic arrivals is about 1 sec). This difference is much less than differences between dominant periods of NTS explosions and Kazakh explosions of similar body-wave magnitude observed at common stations, which were on the average about .4 sec (Springer, personal communication). Simulations performed

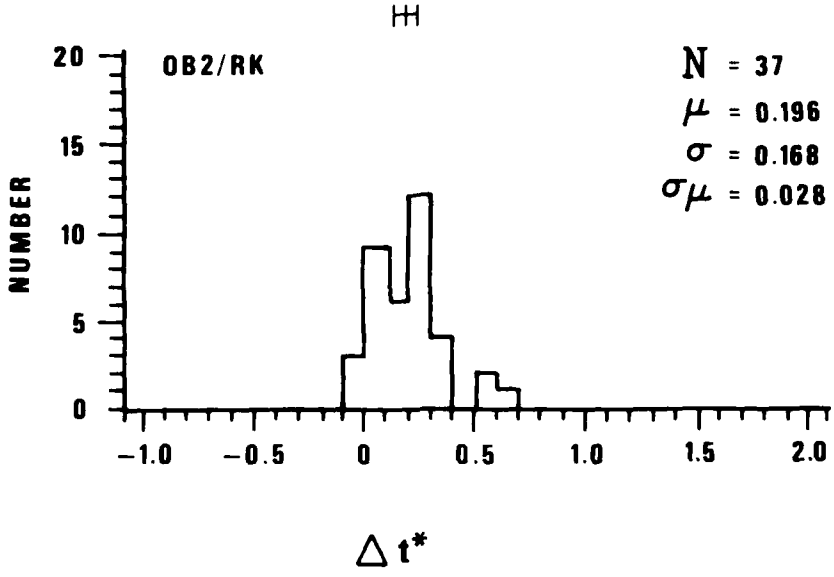

Figure 30. Histogram of Δt* derived from the OB2NV/RKON spectral ratio

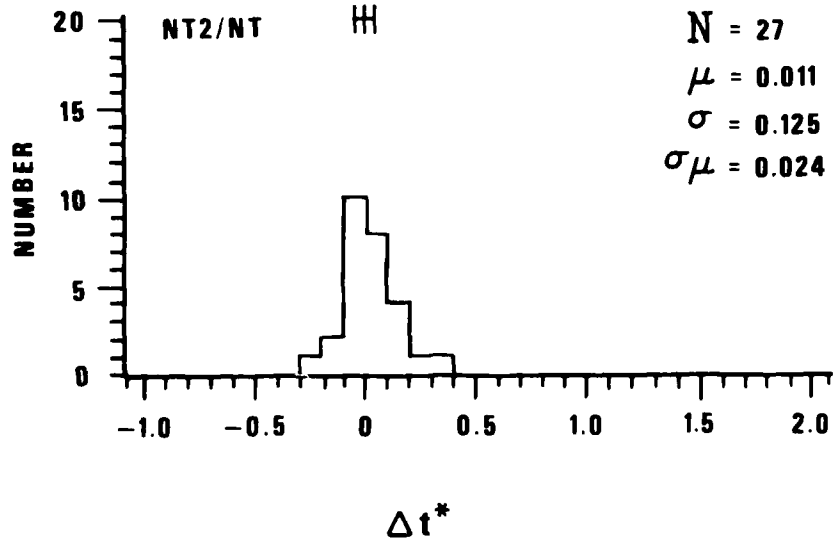

Figure 31. Histogram of Δt* derived from the NT2NV/NTNV spectral ratio

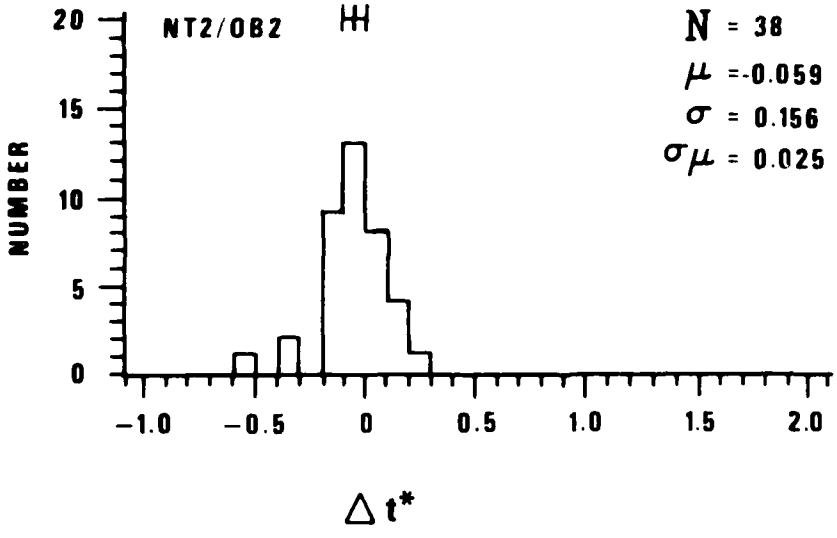

Figure 32. Histogram of Δt^* derived from the NT2NV/OB2NV spectral ratio

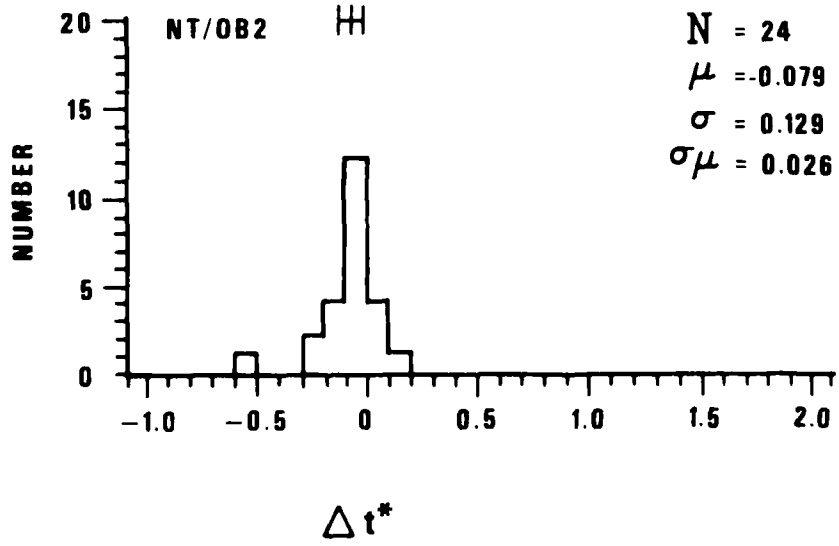

Figure 33. Histogram of Δt^* derived from the NTNV/OB2NV spectral ratio

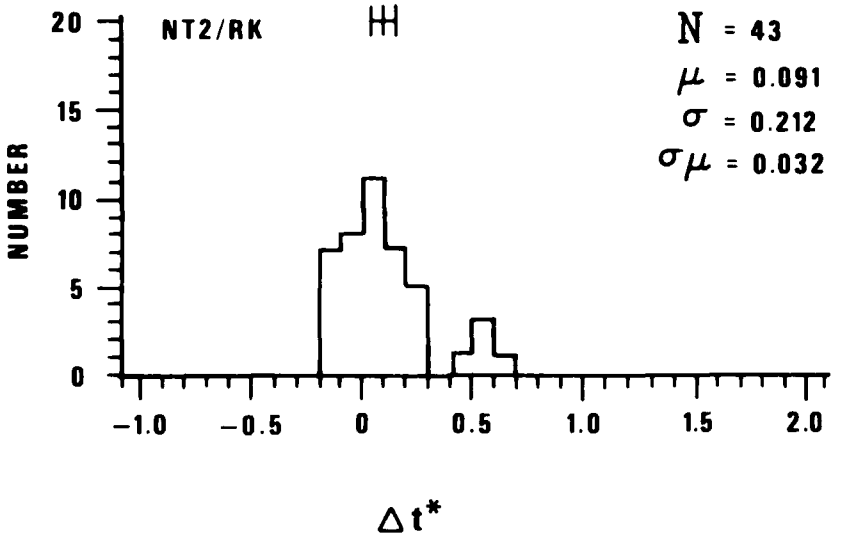

Figure 34. Histogram of Δt* derived from the NT2NV/RKON spectral ratio

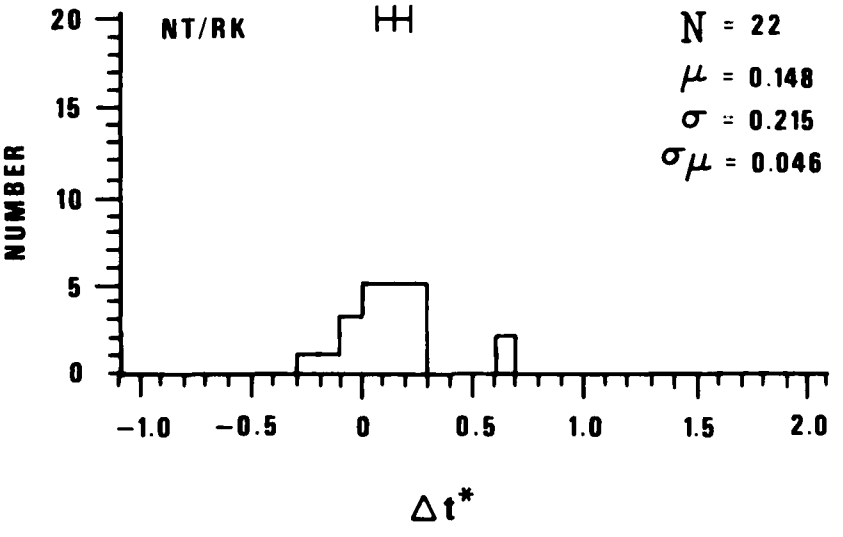

Figure 35. Histogram of Δt* derived from the NTNV/RKON spectral ratio

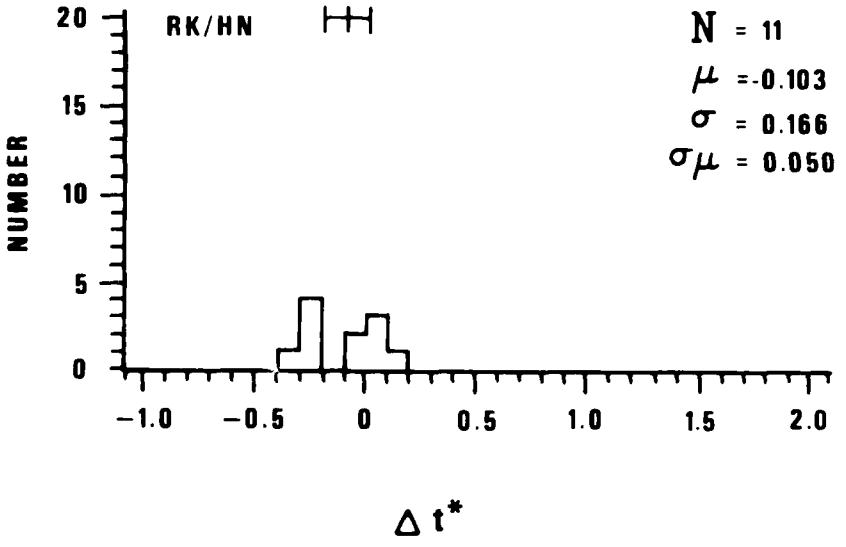

Figure 36. Histogram of Δt^* derived from the RKON/HNME spectral ratio

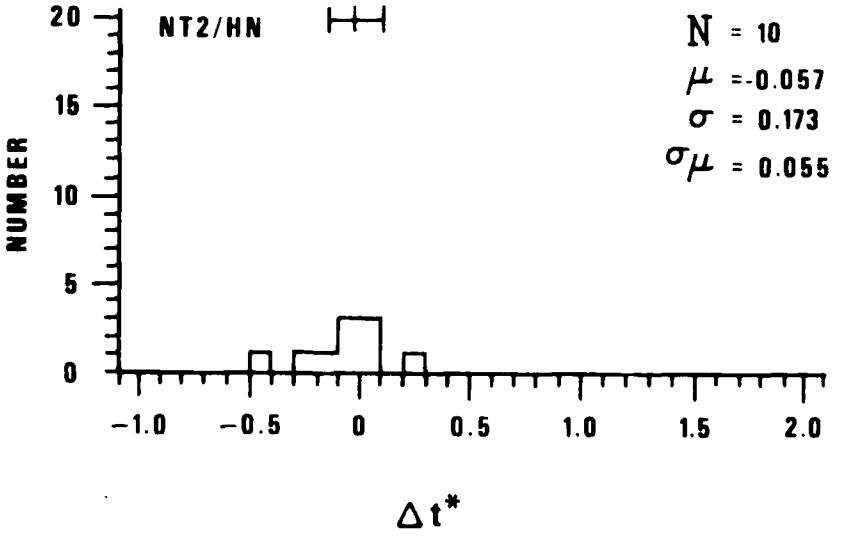

Figure 37. Histogram of Δt^* derived from the NT2NV/HNME spectral ratio

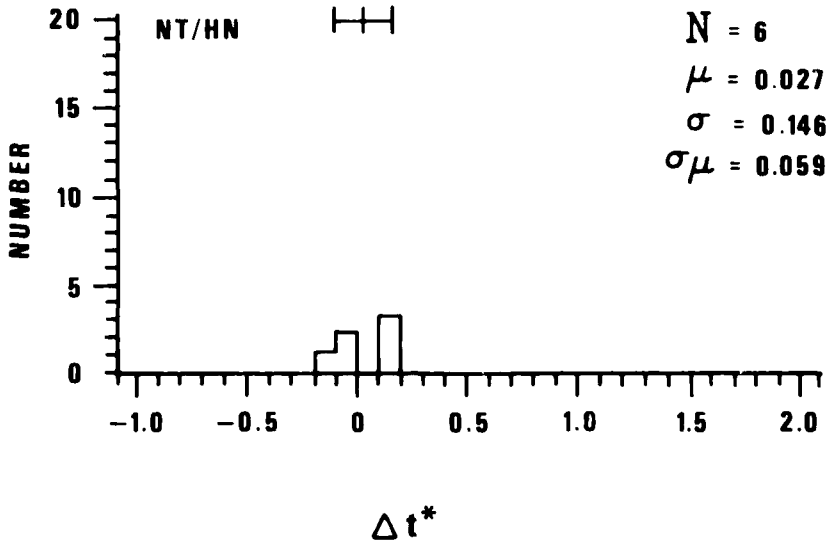

Figure 38. Histogram of Δt* derived from the NTNV/HNME spectral ratio

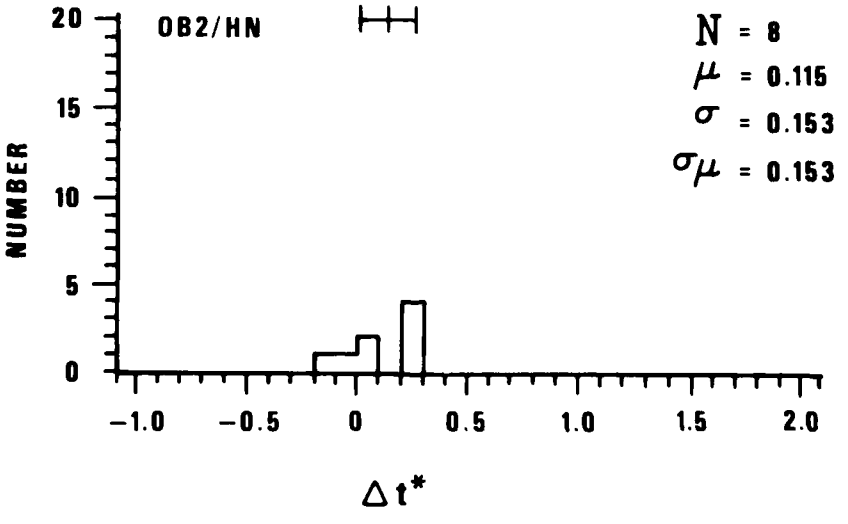

Figure 39. Histogram of Δt* derived from the OB2NV/HNME spectral ratio

TABLE III

Summary of Δt^* Measurements

	STATION PAIR	MEAN	95% CONFIDENCE LIMITS ON MEAN
1.	NT2NV/HNME	-0.057	0.130
2.	NT2NV/RKON	0.091	0.065
3.	NT2NV/OB2NV	-0.059	0.050
4.	NT2NV/NTNV	0.011	0.050
5.	NTNV/HNME	0.027	0.168
6.	NTNV/RKON	0.148	0.098
7.	NTNV/OB2NV	-0.079	0.055
8.	OB2NV/HNME	0.115	0.134
9.	OB2NV/RKON	0.196	0.055
10.	RKON/HNME	-0.103	0.117

on synthetic waveforms (Blandford and Der, 1977; Blandford, 1976) showed that the differential $\Delta t^* \sim .2$, which was postulated between EUS and WUS, could not explain a .4 sec difference in the dominant period, and the differential of dominant periods should have been in the range .1-.2 sec for typical teleseismic arrivals with corner frequencies of around 1.-1.5 Hz. Therefore, most of the .4 sec differential that Springer observed must have been due to causes other than attenuation such as the difference in scale depth of explosions at NTS versus Kazakh or some of the effects of shot media. Thus it is incorrect to attribute the EUS-WUS magnitude differential to the dominant period alone, through the division in A/T. The EUS-WUS magnitude differential, therefore, was mostly the result of amplitude differences, which were significantly lower in the WUS on the 95% confidence level (Der, Massé and Gurski, 1975). The contribution of dominant period to the differential must be less than or roughly equal to .1 magnitude unit.

Procedures Followed in Computing t*

The short-period vertical P wave seismograms, including a noise sample prior to the arrival of the P waves, were anti-alias filtered and digitized from magnetic tape at 20 samples/sec.

A time window comprising 9 sec of the signal and 4 sec of the preceding noise was tapered with a Parzen window and Fourier transformed, and then the power spectrum was computed by multiplying the Fourier spectrum by its conjugate. This power spectrum was then smoothed by a 12-point running average. The shift of the time window was designed to avoid heavy tapering of the first arrival. A noise power spectrum ahead of this window was computed using an identical procedure and subsequently subtracted from the spectrum of the window containing the signal.

Blandford, R. R. and Z. A. Der (1977). Gross characteristics of short-period seismic P waveforms from nuclear explosions as functions of source type, medium, instruments, attenuation, and burial depth. SDAC technical report in preparation, Teledyne Geotech, Alexandria, Virginia 22314.

Blandford, R. R. (1976). Experimental determination of scaling laws for contained and cratering explosions, SDAC, TR-76-3, Teledyne Geotech, Alexandria, Virginia 22314.

The source spectra, determined from scaling or close-in measurements, were then modified with the instrument response and smoothed with a 12-point running average. This procedure was intended to simulate an identical treatment given to the data spectra (the effect of the Parzen window is not very significant relative to the 12-point smoothing). Instead of correcting the spectra for pP or spall, which for any sizeable surface reflection coefficient would introduce spurious peaks into the spectrum, smoothing was relied upon to eliminate any modulation present due to pP or other causes. The fit of straight lines to spectral ratios constitutes, in effect, a final smoothing. We used only the portion of spectrum between .5 and 4. Hz, and in fitting straight lines to the spectral ratios the signal power spectrum was required to exceed the noise by a factor of three. Portions of spectra not satisfying this criterion were not used in the least squares fit. Furthermore, to avoid problems with the dynamic range of the system, the portions of power spectra which were down more than 2.5 orders of magnitude from the peak were also disregarded.

The amplitude spectral ratio was then obtained by taking the square root of the power ratio. Slopes (α) were measured from the graphs, and the values of t* were computed from these by the application of the following formula:

$$t^* = -\frac{\log_e 10}{\pi}\,\alpha$$

ESTIMATION OF THE EFFECT OF LOCAL GEOLOGY

Since the geological structure under the three NTS sites is quite different, the effects of geology on the observed amplitudes must be considered. Stations NT2NV and NTNV are at Pahute Mesa, which is located over a deep volcanic caldera (Silent Canyon caldera) filled with relatively low velocity (α = 3.6 km/sec) tertiary volcanics. The total thickness of these volcanics, tuffs and rhyolite flows is not known, but deep drilling on the Pahute Mesa penetrated the caldera fill to a depth of about 4 km without reaching the bottom of the tertiary volcanic sequence. The OB2NV site, on the other hand, is located on a granite stock which intrudes into high-velocity paleozoic rocks. NT2NV is close to the site of the POOL nuclear explosion while NTNV is located near the KASSERI test site. Some geological information is available from drill holes at both nuclear test sites and crustal models for each SDCS station location were constructed using this information. Table IV gives the crustal models for each station.

The crustal amplification was estimated by computing the vertical displacement for a P wave pulse incident on the models at three angles of incidence, α_i = 20, 25, and 30 degrees measured from the vertical. The pulse used was obtained from the von Seggern-Blandford source model with cube-root scaling, and it has the shape of a far-field displacement from a 50-kt nuclear explosion in granite. The spectrum of this pulse resembles a typical teleseismic arrival with most of the energy below 1 Hz. Figures 40 through 42 show the frequency responses, time domain waveforms, and readings at the three sites.

Table V displays the results of computations. The caldera filling seems to account for about a .2 magnitude increase relative to OB2NV at Pahute Mesa. Correction for this effect brings the amplitudes at Pahute Mesa down to the same level as OB2NV. Because at low frequencies this amplitude variation is expected to vanish, the observed spectrum at Pahute Mesa must be enhanced at high frequencies.

In addition to trying to assess the effects of local geology attempts were also made to find a pattern in the azimuth-distance distribution magnitude residuals, but no consistent behavior emerged. Figures 43a through 43e

TABLE IV

Crustal Models of the Three NTS-SDCS Stations

OB2NV	d (km)	α (km/sec)	β (km/sec)	δ (g/cm^3)
	10.	5.70	3.36	2.70
	10.	6.10	3.60	2.80
	10.	6.70	4.00	2.95
	∞	7.80	4.50	3.30
NT2NV	d	α	β	δ
	1.	2.86	1.75	2.00
	4.	3.60	2.00	2.20
	5.	5.70	3.36	2.70
	10.	6.10	3.60	2.80
	10.	6.70	4.00	2.95
	∞	7.80	4.50	3.30
NTNV	d	α	β	δ
	1.	3.00	1.80	2.00
	4.	3.60	2.00	2.20
	5.	5.70	3.36	2.70
	10.	6.10	3.60	2.80
	10.	6.70	4.00	2.95
	∞	7.80	4.50	3.30

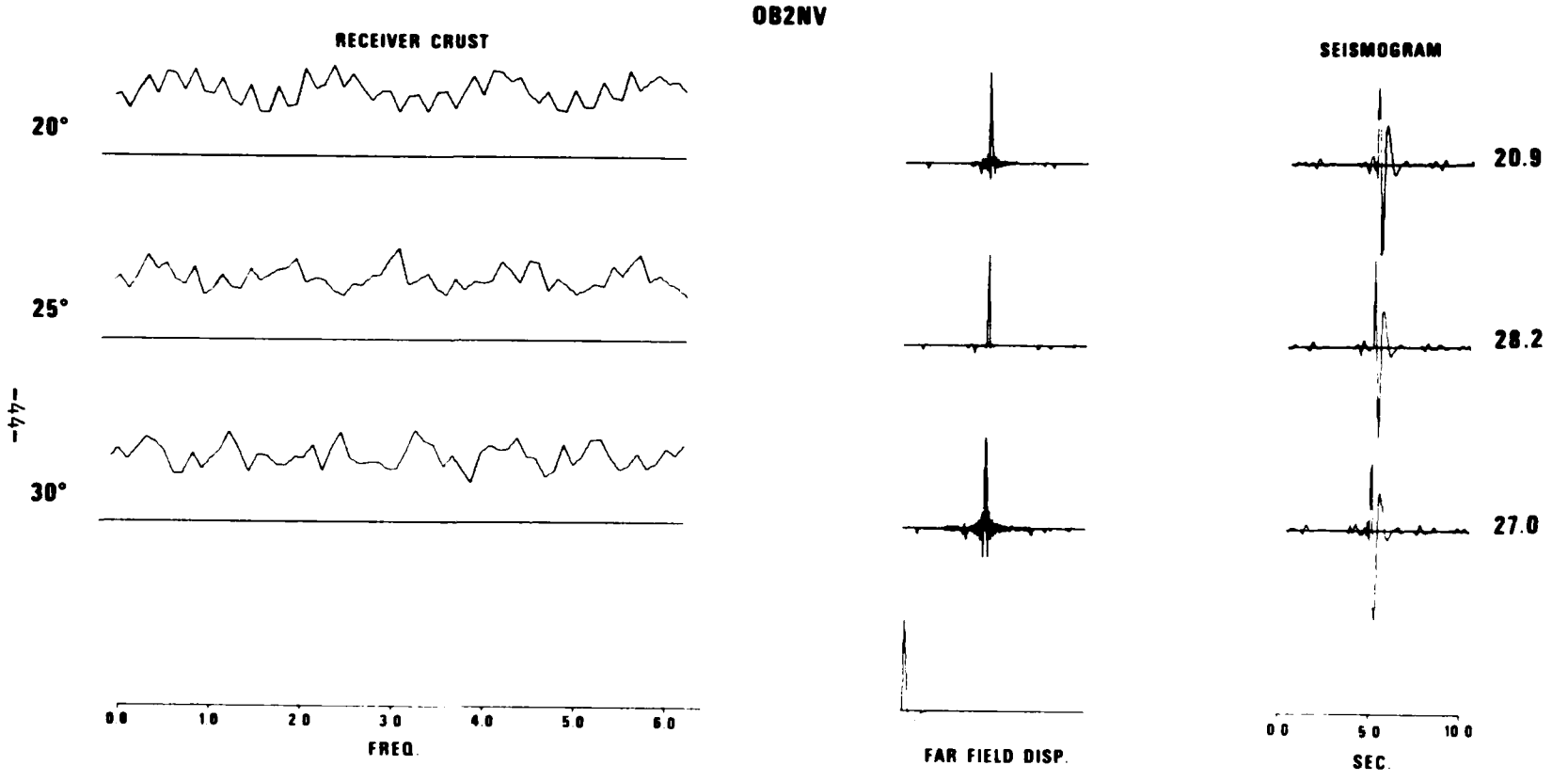

Figure 40. Crustal response calculations at OB2NV

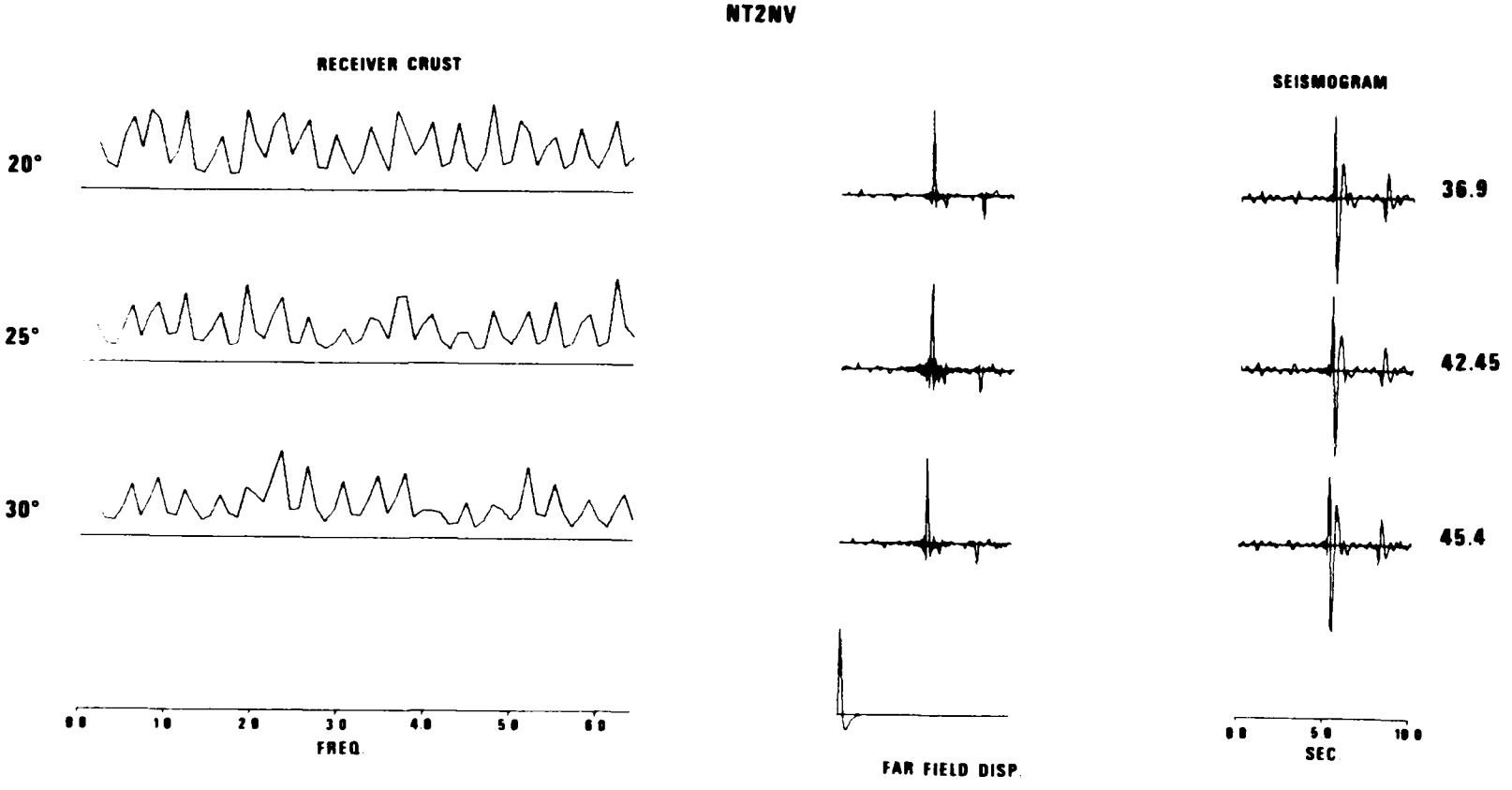

Figure 41. Crustal response calculations at NT2NV

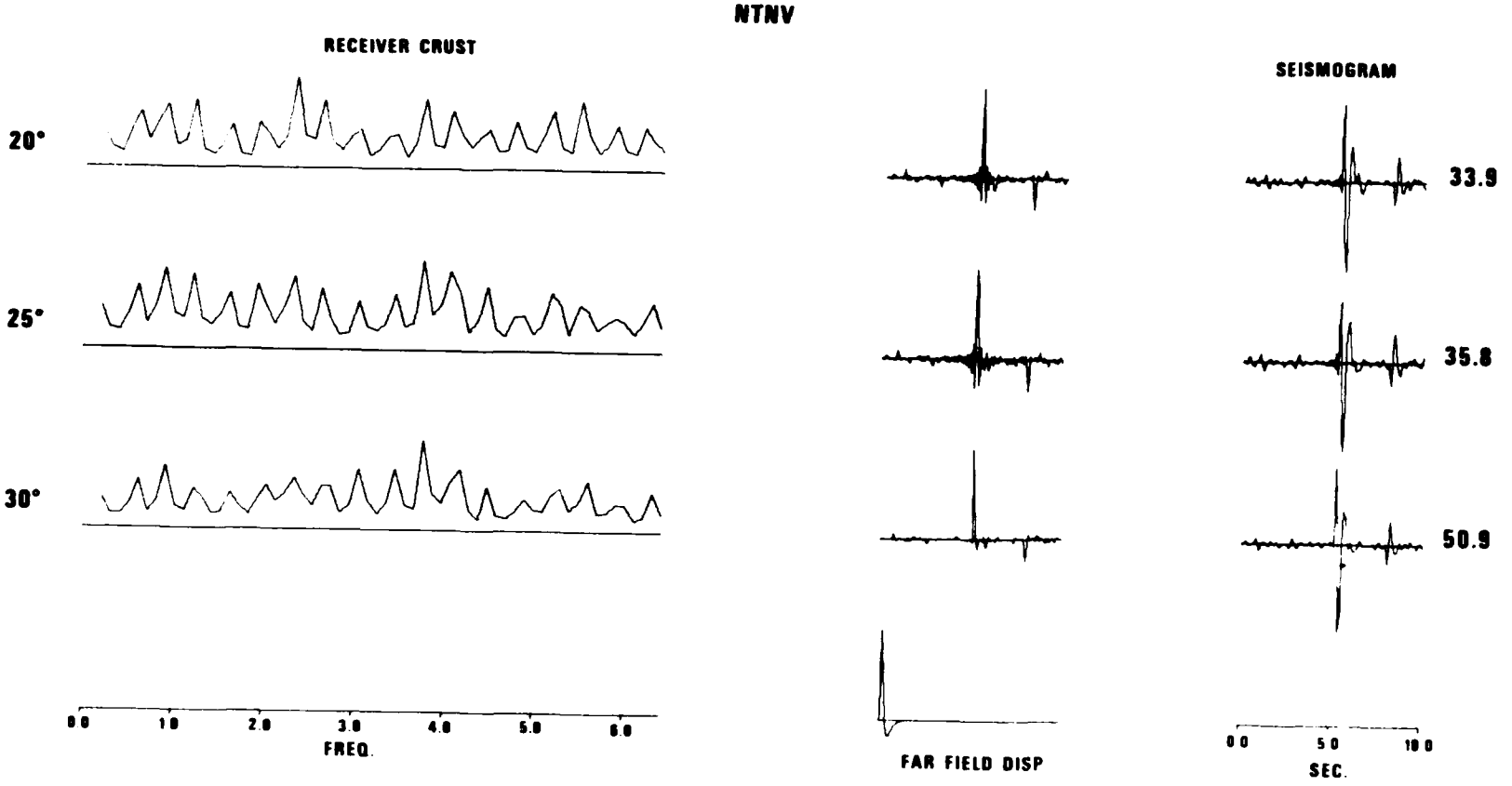

Figure 42. Crustal response calculations at NTNV

TABLE V

Summary of the Differences in Crustal Response
Expressed in Magnitude Units

ANGLE OF INCIDENCE	PULSE AMPLITUDES (Peak to Peak)			AMPLITUDE RATIOS	
	OB2NV	NT2NV	NTNV	NT2/OB	NT/OB
20°	20.9	36.9	33.9	1.77	1.62
25°	28.2	42.5	35.8	1.51	1.27
30°	27.0	45.4	50.9	1.68	1.89
Average pulse amplitude ratios				1.65	1.59
Body-wave residuals relative to OB2NV				.21	.20

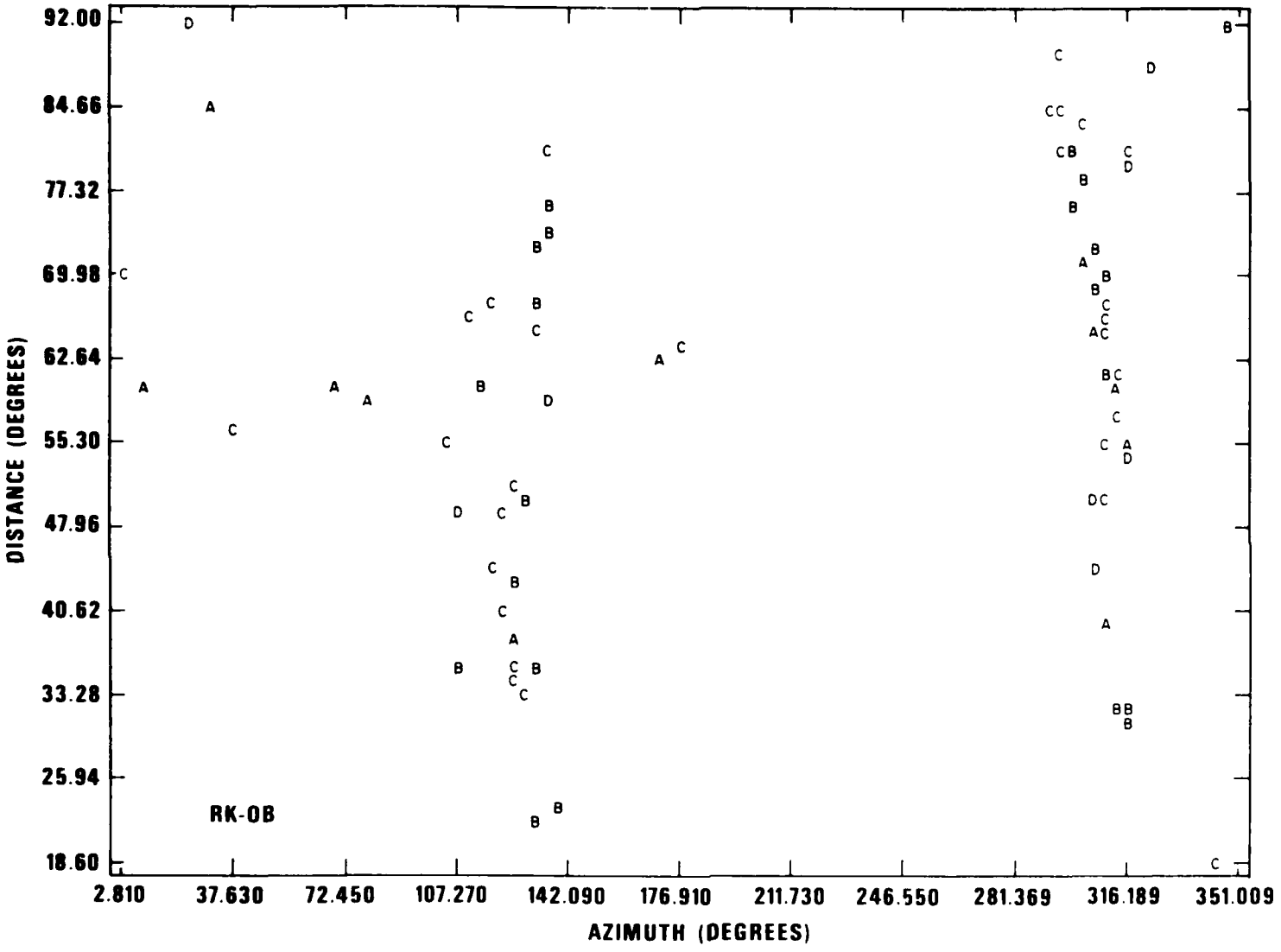

Figure 43a. Azimuth distance plots of magnitude differentials for the station RKON-OB2NV

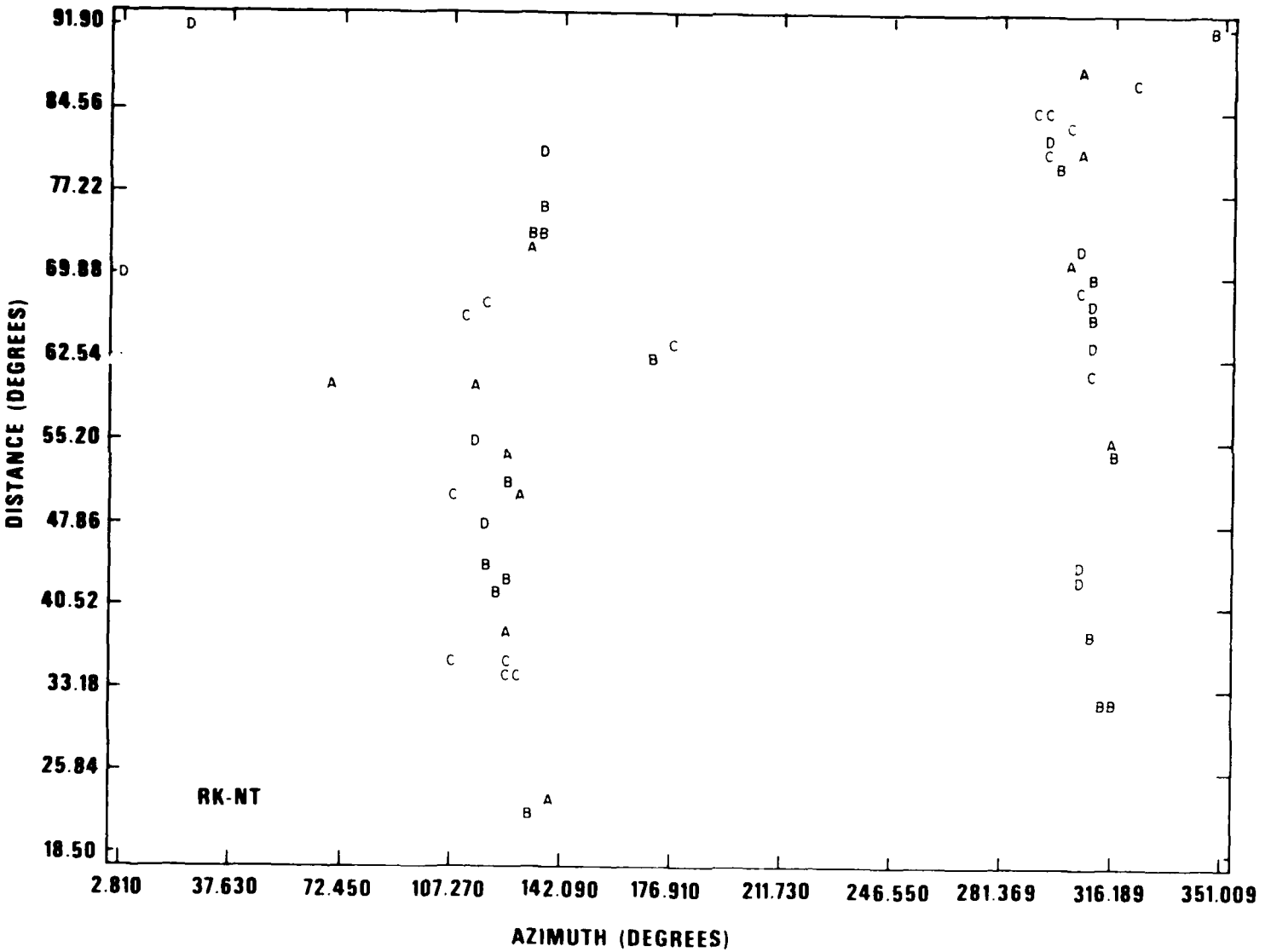

Figure 43b. Azimuth distance plots of magnitude differentials for the station RKON-NTNV

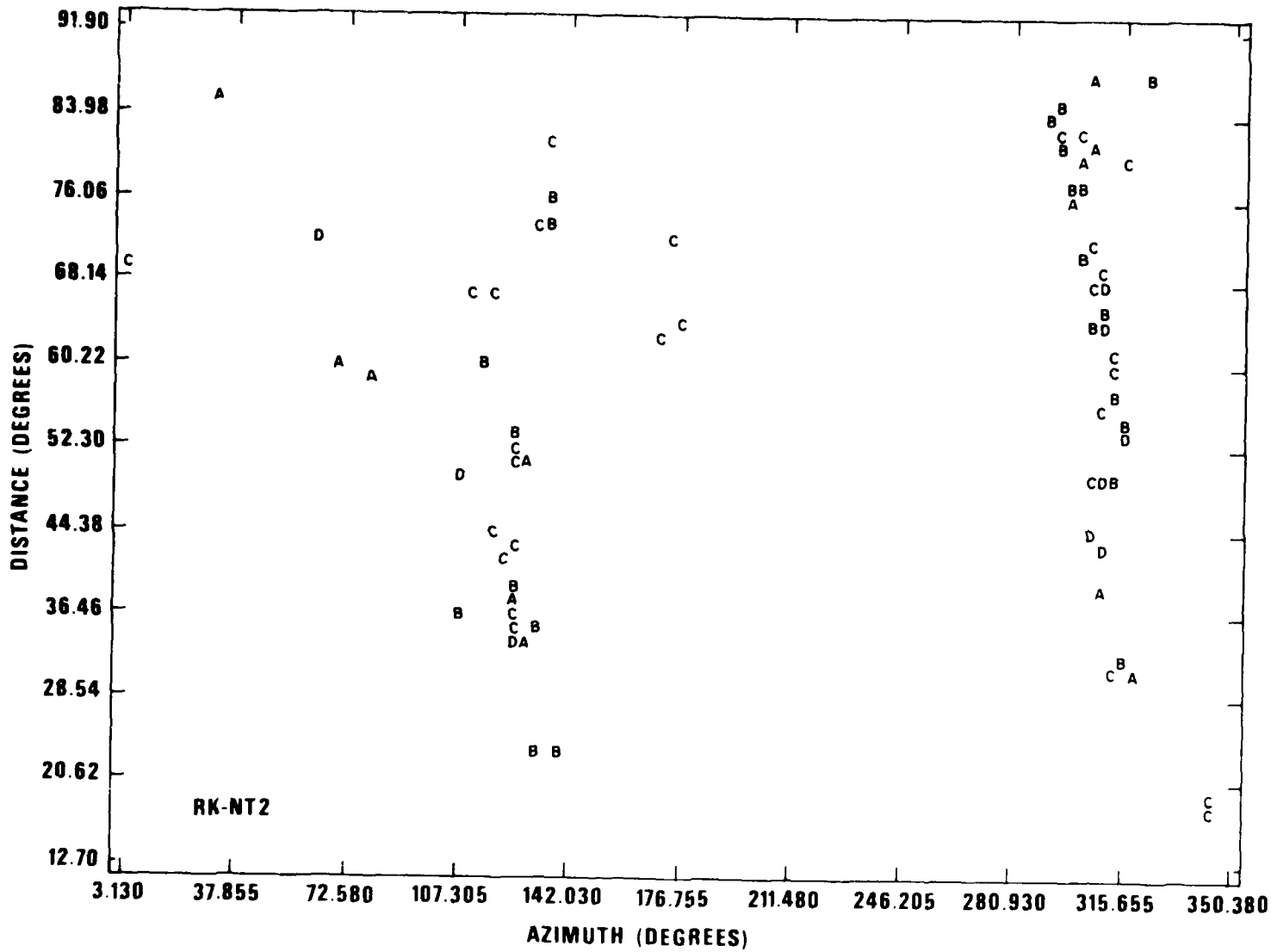

Figure 43c. Azimuth distance plots of magnitude differentials for the station RKON-NT2NV

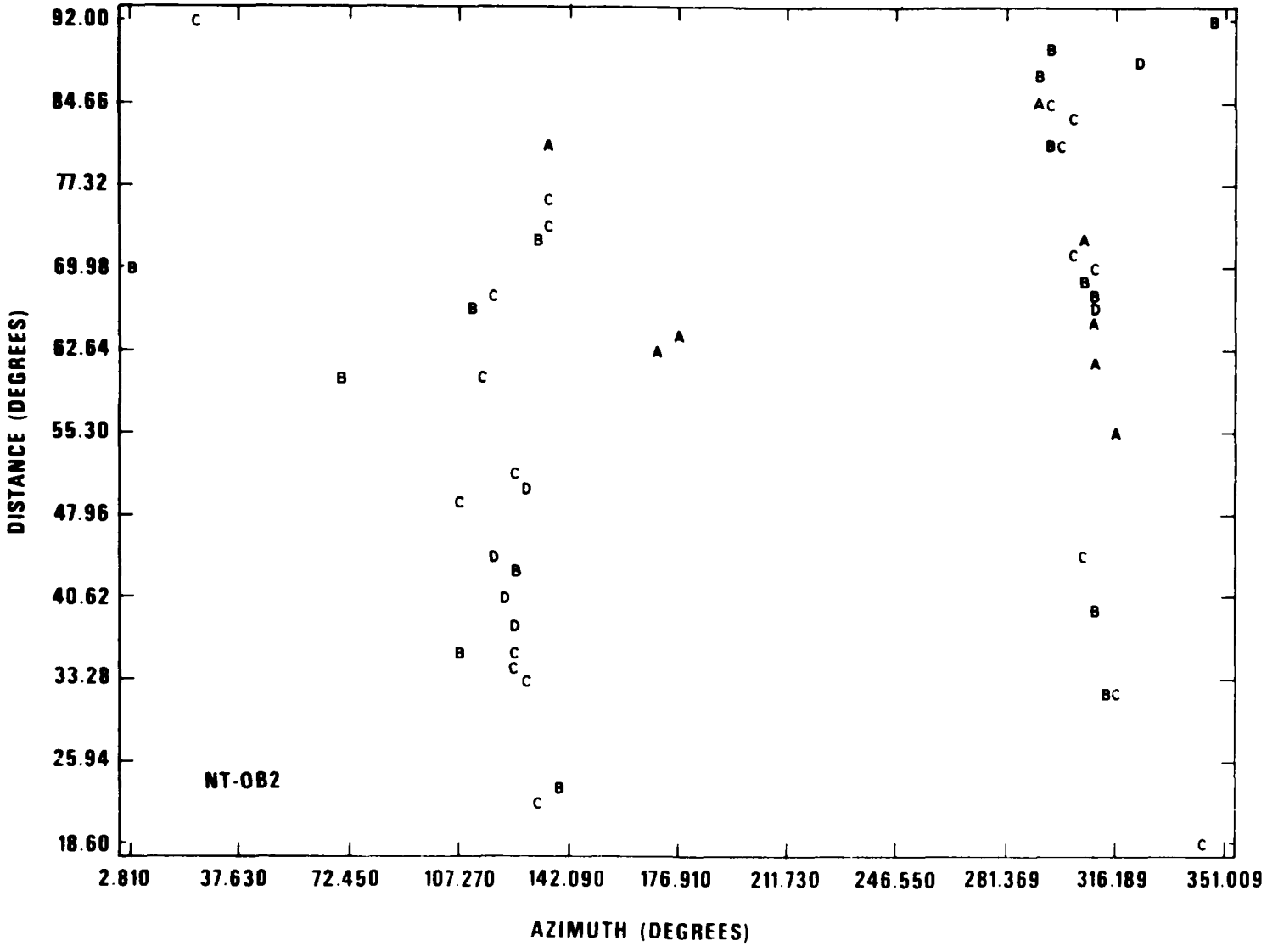

Figure 43d. Azimuth distance plots of magnitude differentials for the station NTNV-0B2NV

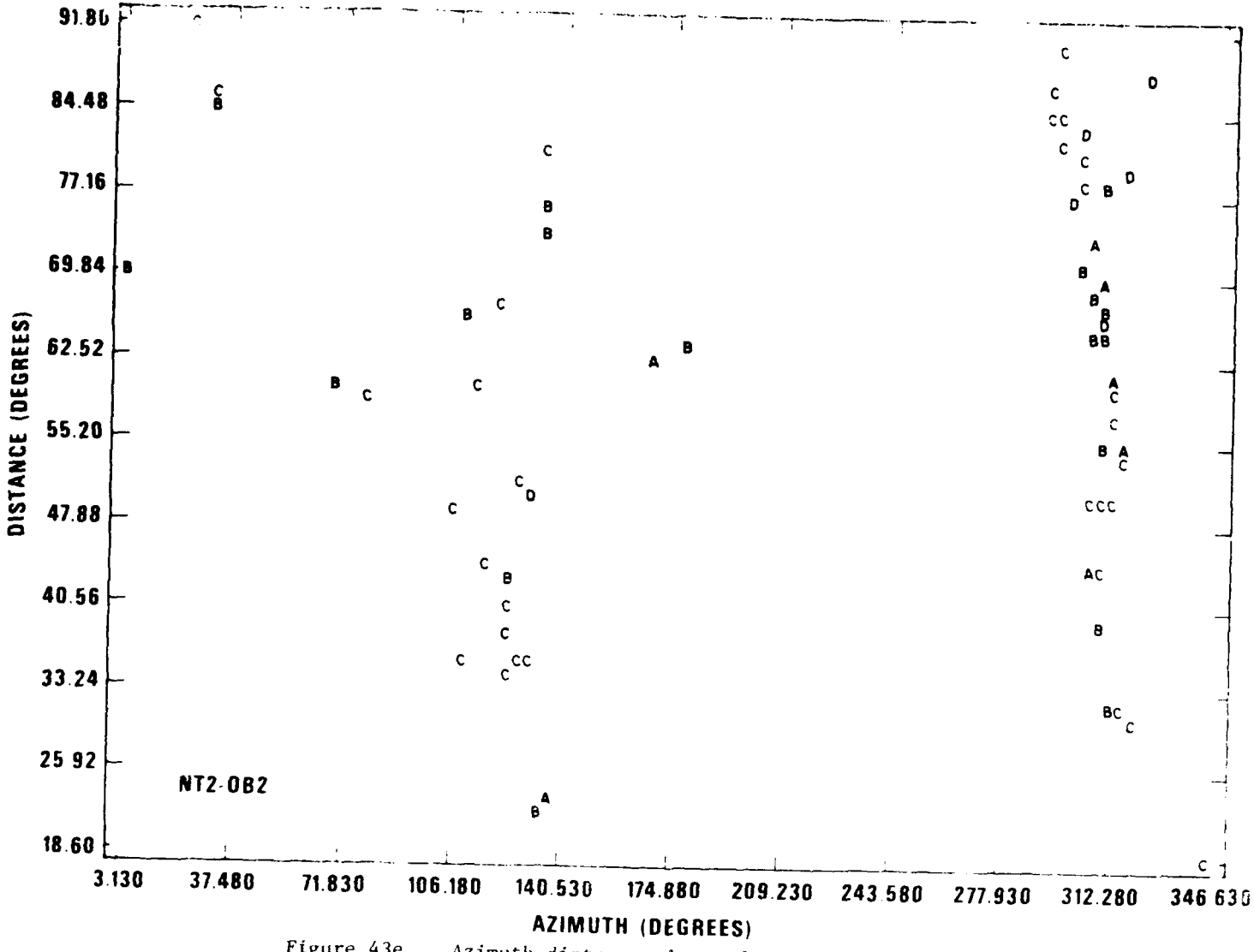

Figure 43e. Azimuth distance plots of magnitude differentials for the station pair NT2NV-OB2NV

show plots of four categories of magnitude differentials Δm_b for various station pairs as functions of azimuth and distance to NTS. The designations are as follows:

A	$(\Delta m_b - \mu) < -\sigma$	(low apparent attenuation at NTS)
B	$-\sigma < (\Delta m_b - \mu) < 0$	
C	$0 < (\Delta m_b - \mu) < +\sigma$	
D	$(\Delta m_b - \mu) > +\sigma$	(high apparent attenuation at NTS)

where μ is the mean and σ is the standard deviation of Δm_b's for the given station pair. No significant effect of distance or azimuth is apparent with the exception of the low-differential "A" events at $\Delta \simeq 600$, $\theta \simeq 40°$, events from the Mid-Atlantic ridge on the azimuth through RKON. These events depart the source at a shallower angle to RKON than to OB2NV and thus the RKON waveforms may suffer more attenuation at the source than do the OB2NV waveforms.

Effect of Attenuation on the m_b Measurement

The low significance of the "uncorrected" magnitude differential between the RKON-OB2NV station pair was an unexpected result of this study. The conventional "corrected" magnitude differential and the differential in t* cannot be distinguished on the 95% confidence level from the regional WUS values established by previous studies with the present accuracy of measurements. Arguments estimating the decrease of amplitude of a single frequency component, 1 Hz, for example, require a decrease of amplitude equivalent to .27 magnitude units. The low significance of the "uncorrected" magnitude differential, however, seems to indicate that no difference exists in amplitudes between RKON and OB2NV.

Re-examination of the method used in computing m_b reveals, however, that "uncorrected" m_b, and conventional m_b as well, is not a suitable measure of the actual amplitudes. The problem of measurement stems from instrument correction that assumes the signal is monochromatic, consisting of a single frequency component with the dominant period T. For a real signal attenuation changes not only the amplitude, but also the period. The mean dominant period of teleseismic arrivals at RKON is about .7 second, while at OB2NV it is about

.9 second. Instrument amplification is higher at .7 second than at .9 second by a factor greater than 1.5. Therefore, "correction" for instrument response tends to restore amplitude at OB2NV that has actually been lost. The correction might be more revealing if it were done in the frequency domain using the same frequency at each station. Dividing by the dominant period T increases the differential for the conventional m_b since T is longer for OB2NV.

Observed magnitude differentials are roughly consistent with the size of Δt^*. Given the subjectivity of picking the "dominant" periods and amplitudes and the approximate nature of "corrections", the noise level of the procedure for computing m_b is similar in size to the biases under study, even if the scatter of body-wave amplitude measurements is disregarded. Since P wave spectra vary considerably no exact functional relationships between the Δt^* and the expected Δm_b can be formulated. This reasoning indicates that one would be better off not using any period dependent instrument correction. Even division by dominant period is a questionable practice.

The magnitude differentials, no matter how poor a measure of energy loss they may be, can be causally related to anelastic attenuation, and are about the size to be expected based on $\Delta t^* \sim .2$. Reciprocity would then imply that signals from NTS would be weakened by about the same amount expressed in m_b units (.18 m.u.).

Travel Time Studies

Although travel times were read for all arrivals that had reasonably good S/N ratio, difficulties were encountered during attempts to find travel-time anomalies. The source of these difficulties was inaccuracies in the locations given in the preliminary event lists used. We concluded that the travel-time study had to be deferred until better locations and depths are computed using the maximum number of available stations. The ISC list, when updated, may provide such improved locations.

Bias Due to Unequal Thresholds at the Various SDCS Stations

Since the noise levels of stations used in this study vary widely, there is a danger that the unequal noise levels will change the effective bias

differences measured. The mean of magnitudes measured near the noise level tends to be higher in value than the actual or true value (Herrin and Tucker, 1972; von Seggern and Blandford, 1976). Although only events with good signal-to-noise ratio were measured, the danger still exists that our S/N criteria will bias Δm_b determinations. Plots of Δm_b against magnitude, however, do not show any clear trend (Figure 44), and we are reasonably confident that there is no appreciable bias due to varying thresholds. Moreover, our threshold is also constrained by the event list used, since we looked for already detected events only.

Evaluation of Attenuation Under the SHOAL Site

The 12.5 kt contained nuclear explosion, SHOAL, was detonated in a granite body in western Nevada. The purpose of the SHOAL project was to compare seismic radiation from this explosion with earthquakes in the same area (Fallon earthquakes). The LRSM station SZNV was operated from 5 January 1963 to 8 February 1963 and was located about six hundred feet north of the ground zero of SHOAL, on the same granite body where the nuclear device was emplaced. The existence of station SZNV offered an opportunity to compute attenuation under this test site by comparing spectra of P waves observed here to those recorded at a station on a stable platform (shield) type structure. The site selected for comparison is Sleepy Eye, Minnesota (SEMN), also on granite. The standard procedure described above was followed for the computation of spectral ratios for these stations.

Figures E1 to E21 of the Appendix show the vertical SP waveforms, power spectra (uncorrected for instrument response), and the amplitude spectral ratios with straight-line fits for the 21 teleseismic events which had the best signal-to-noise ratios during the existence of SZNV. Epicentral data for these events are given in Table VI. The signal-to-noise ratios of these events are still quite variable so, due to the built-in signal-to-noise ratio

Herrin, E. and W. Tucker (1972). On the estimation of body-wave magnitudes, Report to AFOSR, Dallas Geophysical Observatory, Southern Methodist University, Dallas, Texas.

von Seggern, D. H. and R. R. Blandford (1976a). Seismic threshold determination, Bull. Seism. Soc. Am., 66, 753-788.

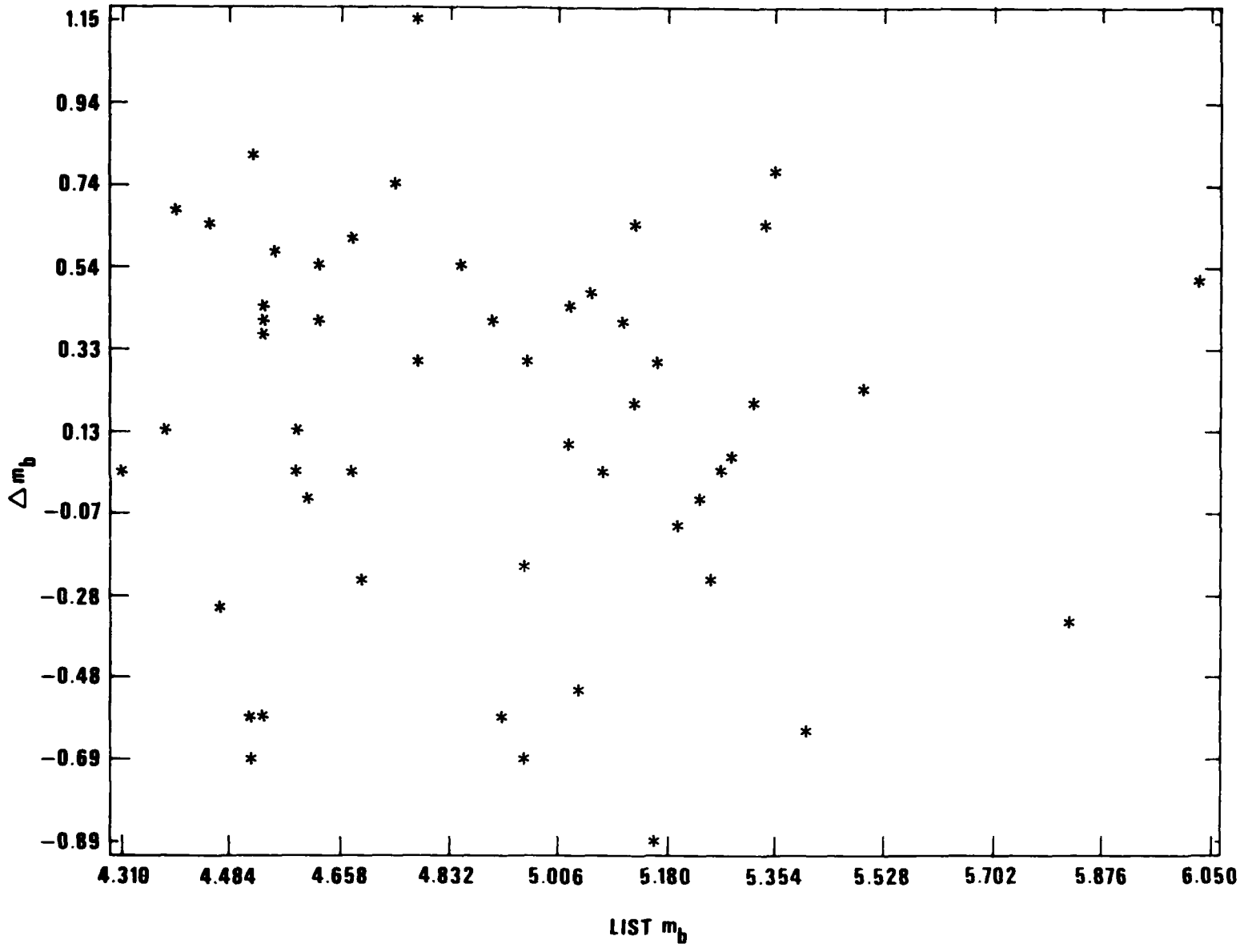

Figure 44. m_b vs. List m_b for the RKON–OB2NV station pair

TABLE VI

Summary of Δt* Determinations for the LRSM Station Pair SEMN/SZNV

EVENT DATE	REGION	LAT.	LONG.	ORIGIN TIME	ARRIVAL SEMN	ARRIVAL SZNV	Δt*
05 Jan 63	W. Brazil	7.1S	71.6W	17 43 33.1	17 52 17.	17 53 07.	.057
08 Jan 63	Japan	31.3N	130.3E	15 46 44.1	15 59 46.	15 59 04.	-.377
11 Jan 63	Coast of S. Chile	44.9S	75.9W	12 12 16.9	12 25 16.	12 25 25.	-.081
12 Jan 63	Columbia	4.7N	76.7W	03 40 33.1	03 48 27.	03 49 32.	.204
13 Jan 63	Argentina	32.0S	69.2W	17 20 21.6	17 32 19.	17 32 45.	.290
16 Jan 63	Aleutians	51.4N	179.7W	05 44 54.4	05 54 16.	05 52 53.	.002
16 Jan 63	North Atlantic	54.2N	35.1W	12 32 37.1	12 40 00.	12 42 10.	.140
16 Jan 63	Chile-Arg Border	23.9S	67.7W	15 09 11.4	15 20 21.	15 20 59.	.539
21 Jan 63	Chile-Arg Border	34.5S	70.5W	04 15 43.3	04 27 51.	04 28 10.	.169
21 Jan 63	Kamchatka	53.3N	157.4E	04 25 04.6	04 35 43.	04 34 37.	.325
27 Jan 63	E. Caucasus	40.9N	49.7E	19 35 16.3	19 48 02.	19 48 50.	.405
28 Jan 63	Peru	11.2S	76.9W	02 12 13.3	02 21 52.	02 22 30.	.285
28 Jan 63	Japan	43.7N	144.7E	04 05 31.6	04 17 28.	04 16 36.	.030
28 Jan 63	Alaska Pen.	54.7N	161.7W	13 00 48.1	13 08 49.	13 07 20.	.351
29 Jan 63	Kuriles	49.8N	155.0E	09 21 16.2	09 32 03.	09 31 05.	.182
31 Jan 63	E. China Sea	27.1N	126.7E	05 06 43.4	05 20 22.	05 19 40.	.288
05 Feb 63	Aleutians	53.7N	165.5W	12 08 20.5	12 16 40.	12 15 11.	.063
05 Feb 63	Coast of Mexico	15.3N	94.2W	17 49 57.3	17 55 48.	17 56 06.	-.215
05 Feb 63	Coast of Chile	38.5S	73.5W	20 39 20.4	20 51 52.	20 52 07.	.707
06 Feb 63	North Columbia	6.8N	73.2W	03 27 56.9	03 35 40.	03 36 56.	.169
06 Feb 63	Komandorsky	55.7N	166.2E	18 17 11.3	18 27 09.	18 26 09.	.154

criteria in our computational procedure, the frequency range of the signal spectral ratios used for determining Δt^* is also variable. While eighteen spectral ratios (SZNV/SEMN) have a negative slope, indicating less high frequency content for P waves at SZNV, only three spectral ratios have a positive slope. The relative lack of high frequencies at SZNV is quite visible on most signals in the time domain, where SZNV waveforms have broader pulses and less high frequency riding on the signals. In some cases, such as the 16 January 15:09:11.4 GMT, 5 February 20:39:20.4 GMT, and 6 February 03:27:56.9 GMT events, the effect is quite dramatic. In other cases there is no clearly visible difference (16 January 05:44:54.4 GMT).

A notable "counter example" is the 8 January 15:46:44.1 event that showed a broad pulse at the arrival time of the P wave at SEMN. Examination of film records of this event, however, show highly unstationary, high amplitude, pulsing long-period noise ahead of the signal (a similar pulse is shown just ahead of the signal). Thus, the possibility that the waveform shown is a super-position of a long-period noise pulse and the actual higher frequency signal cannot be ruled out.

One possible source of error in the determination of Δt^* might be frequency dependent radiation patterns for the events used. However, only one of the events (29 January 09:21:16:.9 GMT) shows first motions with different polarities at the two stations. For the remaining events both stations are on the same lobe of the radiation pattern as indicated by first motions or the general matching character of the wave-trains. Though most events occurred along the circumpacific seismic belt, which can introduce preferred orientations of the focal mechanisms relative to the stations used, the likelihood of this situation causing a significant bias is low because a variety of focal mechanisms exists in these regions. In addition, the two events not along the NNW-SSE azimuths that are characteristic of circumpacific events show similar Δt^* values.

Table VI displays the Δt^* values derived from the spectral ratios. The mean of all values in the table is $\Delta t^* = .18 \pm .10$ (95% limits), which explains the EUS versus WUS magnitude bias of .25 magnitude units at 1 Hz. These values are of the same order as other determinations of the regional WUS-EUS

magnitude bias and Δt^* (Der and McElfresh, 1976; North, 1976; Booth, Marshall and Young, 1974).

Observations of seismic waves from the nuclear explosion SHOAL helps to solve the reciprocal problem and to compute the attenuation of P waves to various North American stations. The source spectrum used for computing spectral ratios was obtained by scaling up the standard 5 kt granite source spectrum (von Seggern and Blandford, 1972) using cube-root scaling. Because of the relatively small difference in yield, the spectrum does not change radically, even if this scaling law is not strictly valid (Der and McElfresh, 1976). The source power spectrum used, which includes the LRSM system response, is shown at the top of Figure 46.

Figures 45 through 47 display seismic traces, power spectra (not corrected for instrument response), and station-to-source amplitude spectral ratios with least squares straight-line fits. Table VII provides the slopes and the corresponding t* values. Most of the values are above .4; only one, HNME, is unexpectedly low. The average of all values is .42, which is in fairly good agreement with other shield-WUS type paths (Der, 1976).

The average .42 for shield to SHOAL site combined with the SZNV-SEMN differential $\Delta t^* \sim .18$ yields the absolute average t* of .24 for shield-to-shield type paths. This value is again in very good agreement with past work and other data from the literature that Der (1976) summarized.

Spall and pP can change this source spectrum. The measured uphole time at SHOAL was about .08 sec, yielding a two-way time of .16 sec which translates into a 6.25 Hz first null of the spectrum for total reflection. This figure is beyond the frequency range of our computations. The effect of such

---

Der, Z. A. and T. W. McElfresh (1976a). Short-period P wave attenuation along various paths in North America as determined from P wave spectra for the SALMON nuclear explosion, Bull. Seism. Soc. Am., 66, 1609-1622.

von Seggern, D. H. and R. R. Blandford (1972). Source-time functions and spectra for underground nuclear explosions, Geophys. J. R. Astr. Soc., 31, 89-97.

Der, Z. A. (1976). On the existence, magnitude and causes of broad regional variations in body-wave amplitudes (magnitude bias), SDAC-TR-76-8, Teledyne Geotech, Alexandria, Virginia 22314.

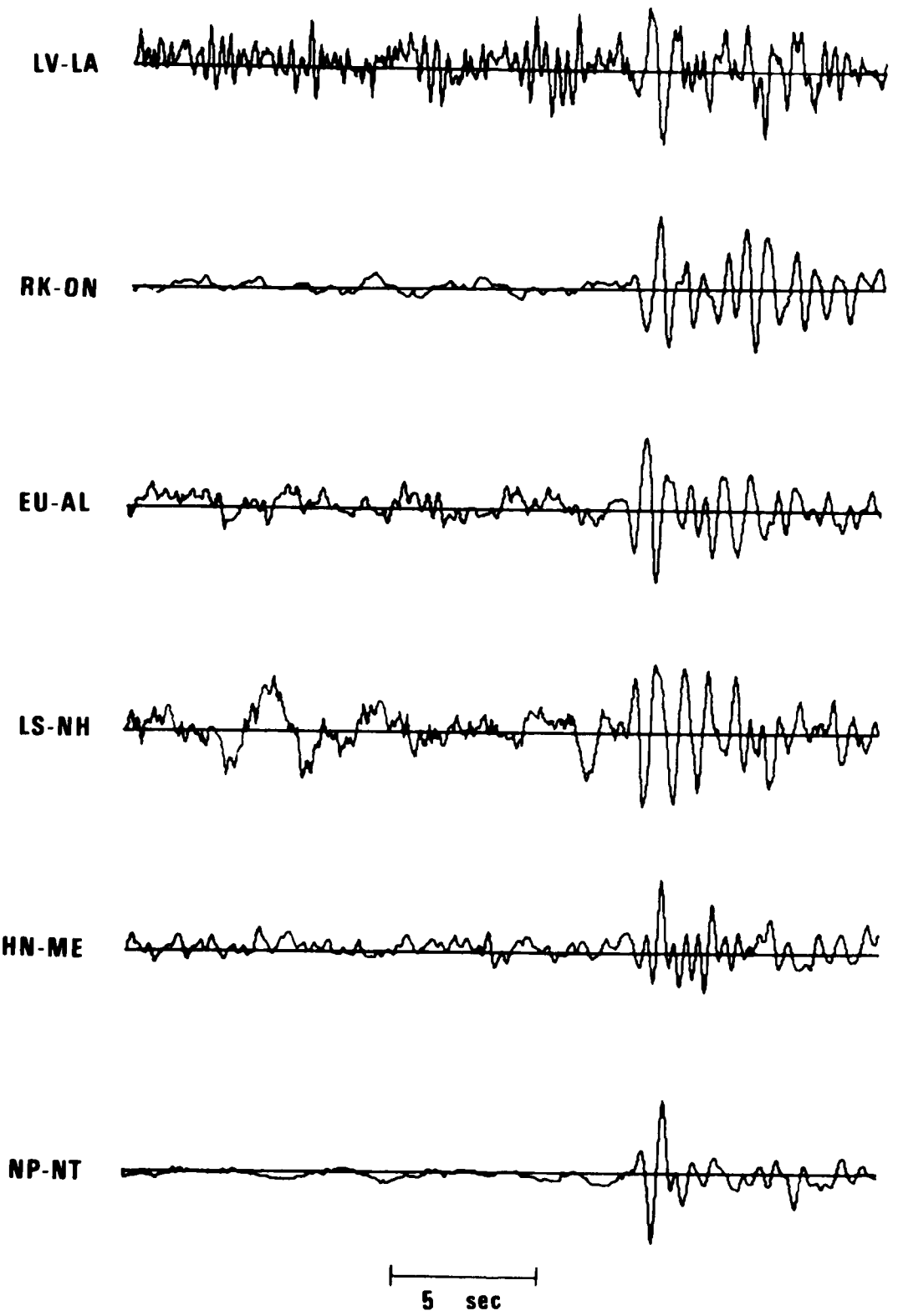

Figure 45. Vertical component P waveforms of the SHOAL nuclear explosion at selected LRSM sites

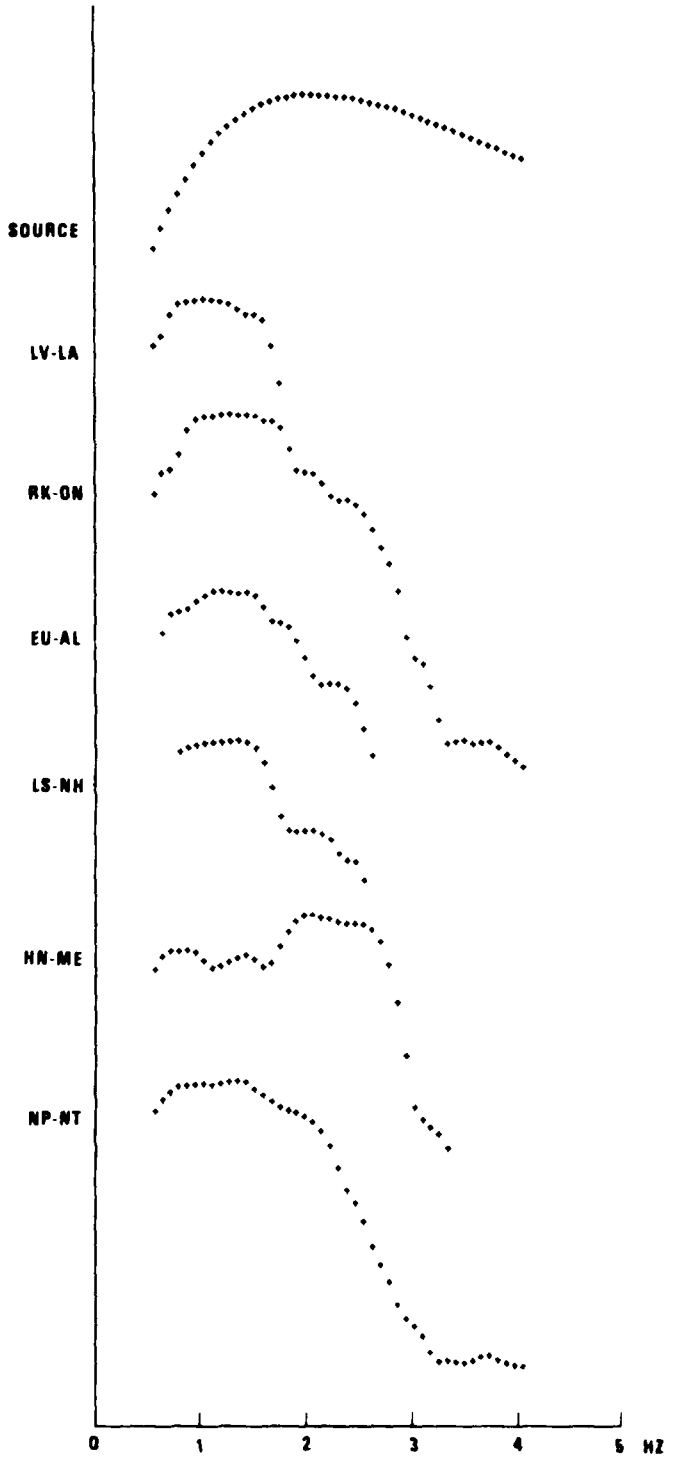

Figure 46. P wave power spectra (uncorrected for instrument response) of P waves from SHOAL. The estimated source spectrum of SHOAL, also modified by the instrument response, is shown on the top of the figure.

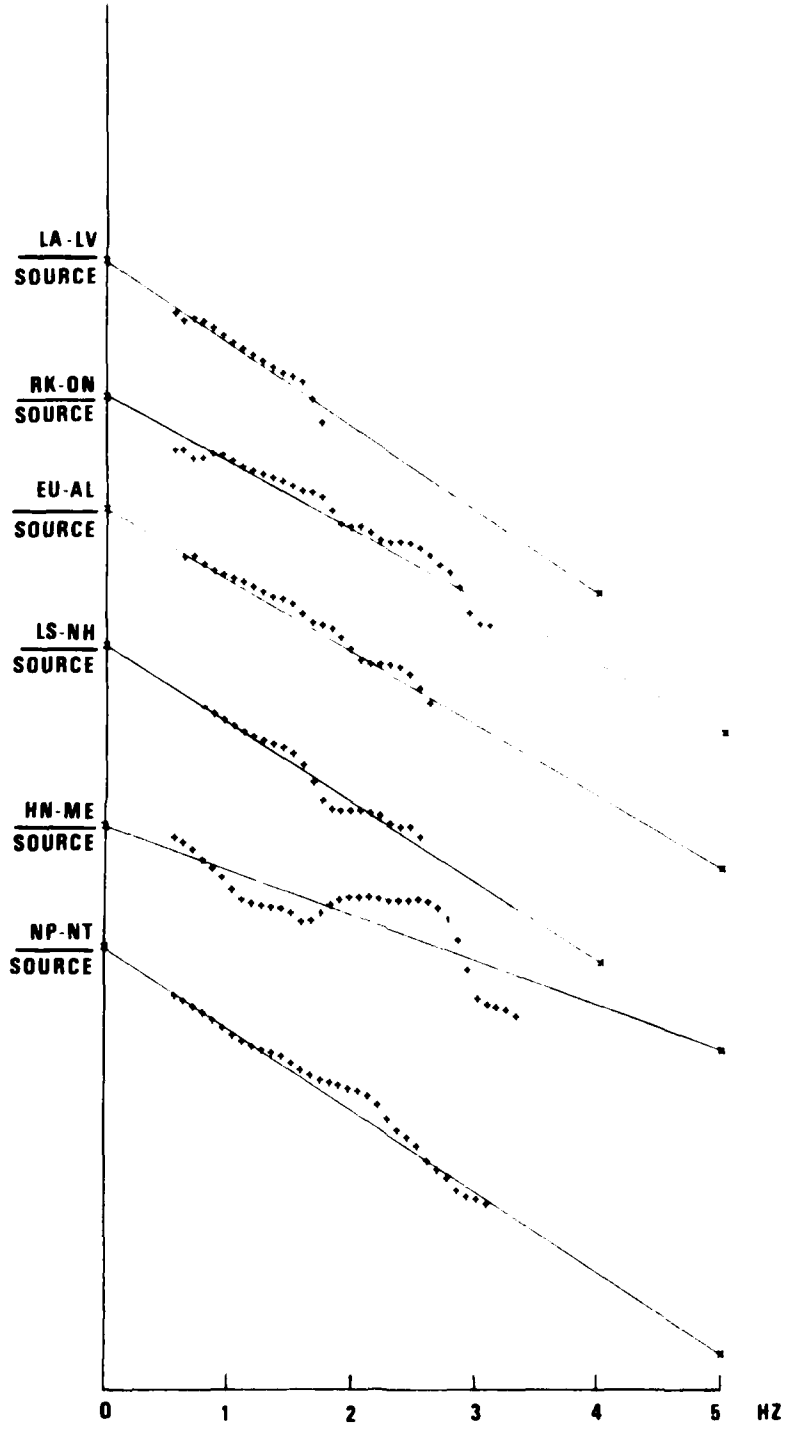

Figure 47. Station-to-source amplitude spectral ratios for SHOAL.

TABLE VII

Absolute t* Values along Paths from
The SHOAL Nuclear Explosion to Selected LRSM Stations

STATION	α SLOPE	$t^* = \frac{-\log_e 10}{\pi} \alpha$
NPNT	-.657	.48
RKON	-.548	.40
LVLA	-.675	.49
EUAL	-.581	.43
LSNH	-.646	.47
HNME	-.360	.26
	Average	.42

modification in spectra, if not considered, would produce a slight decrease of t* values. Thus, t* values could be higher than given here.

Vertical acceleration records show a free-fall time at the surface ranging from .35 to .45 seconds at some of the close-in stations. Oddly, station 10 close to ground zero showed little spall. The free-fall times read from the various accelerometer records, augmented with additional delays (only approximately known) stemming from the two-way travel time of impulses between the shot and the free (or spall) surface, yielded delay times in the range of .35 to .65 second. Delays of such magnitude will introduce at least two or three maxima-minima modulation cycles in the spectra within the frequency range used here. The smoothing applied and the straight-line fitting to spectral ratios will minimize the effect of such modulations on the attenuation measurements. In addition, the sharp fall-off of the spectra with frequency cannot be attributed either to spalling or pP modulation; thus, it results from attenuation.

Analysis of the LRSM Stations EKNV and CUNV

To see the characteristics of P waves in a wider area of Basin and Range near NTS, recordings were read of teleseismic P waves at LRSM stations EKNV and CUNV; RKON was used for reference in eastern North America. While EKNV was operational for many years, CUNV was occupied for only seven months. Table VIII lists the 39 events, readings, and magnitudes at all stations. Two of the events were excluded from further analysis because their epicentral distances are less than 25°. This section of the study is aimed at establishing the existence of magnitude or spectral differences between RKON and the two Basin Range stations. Figure 48 and 49 show histograms of the magnitude differentials involved. Both are significant at the 95% confidence level, indicating that magnitudes at CUNV ($\Delta m_b = -.284 \pm .187$) and EKNV ($\Delta m_b = -.267 \pm .104$) are lower than at RKON. The "uncorrected" magnitude differentials (Figures 50 and 51) are also statistically significant at EKNV ($\Delta m_b^{unc} = -.201 \pm .116$), indicating that low-frequency amplitudes are also significantly lower; the RKON dominant periods are significantly shorter ($\Delta T = .133 \pm .075$) than at EKNV (Figure 52). At CUNV the sign of the mean difference in periods also indicates longer P wave periods than those observed at RKON (Figure 53), but

TABLE VIII

Events used and readings at LRSM stations CUNV, EKNV, and RKON.

1 15 11 63 21: 6:34.0 KURILES

STA	DIST	AMP	T	LOG10(A/MT) + B MB	LOG10(A/M) + B MB
CU-NV	67.5	152.5	1.10	5.97	6.01
EK-NV	67.0	238.1	0.80	5.96	5.87
RK-ON	70.5	606.8	0.80	6.27	6.17
HN-ME	83.8	278.0	0.60	5.98	5.75

2 16 11 63 6:46:15.7 CHILE

STA	DIST	AMP	T	LOG10(A/MT) + B MB	LOG10(A/M) + B MB
CU-NV	83.9	77.1	1.60	5.98	6.18
EK-NV	84.5	42.9	1.50	5.67	5.85
RK-ON	92.3	116.4	1.10	5.98	6.02
HN-ME	89.2	96.2	1.20	5.84	5.92

3 18 11 63 14:38:28.9 CALIFORNIA

STA	DIST	AMP	T	LOG10(A/MT) + B MB	LOG10(A/M) + B MB
CU-NV	8.9	475.6	0.90	5.60	5.55
EK-NV	9.5	139.8	0.70	4.90 ** OMITTED **	4.84
RK-ON	25.7	556.9	1.80	6.37	6.62
HN-ME	38.8	211.5	1.40	5.73	5.87

4 19 11 63 11: 0:54.3 KURILES

STA	DIST	AMP	T	LOG10(A/MT) + B MB	LOG10(A/M) + B MB
CU-NV	67.3	126.0	1.10	5.89	5.93
EK-NV	66.8	126.6	1.30	6.02	6.14
RK-ON	70.3	573.5	0.80	6.24	6.15
HN-ME	83.6	329.6	0.70	6.06	5.91

5 21 11 63 21: 1:35.3 KURILES

STA	DIST	AMP	T	LOG10(A/MT) + B MB	LOG10(A/M) + B MB
CU-NV	60.2	36.6	1.10	5.17	5.21
RK-ON	62.7	113.7	0.80	5.57	5.47
HN-ME	76.2	119.7	0.90	5.60	5.56

6 28 11 63 15:13:11.0 ALEUTIANS

STA	DIST	AMP	T	LOG10(A/MT) + B MB	LOG10(A/M) + B MB
EK-NV	48.6	40.8	0.80	5.04	4.94
RK-ON	53.2	277.5	0.90	5.79	5.74
HN-ME	69.1	115.8	0.80	5.65	5.55

7 3 12 63 23: 3:41.6 CHILE

STA	DIST	AMP	T	LOG10(A/MT) + B MB	LOG10(A/M) + B MB
CU-NV	74.8	414.6	1.10	6.20	6.26
EK-NV	75.3	233.3	1.10	5.98	6.02
RK-ON	76.3	363.8	0.80	6.05	5.95
HN-ME	68.6	322.0	1.20	6.36	6.44

8 10 12 63 14:49:42.6 CHILE

STA	DIST	AMP	T	LOG10(A/MT) + B MB	LOG10(A/M) + B MB
CU-NV	71.8	109.1	0.80	5.52	5.43
EK-NV	72.3	116.8	0.90	5.59	5.55
RK-ON	72.4	69.6	0.80	5.32	5.23

TABLE VIII (Continued)

Events used and readings at LRSM stations CUNV, EKNV, and RKON.

9 11 12 63 0:47:48.3 **TONGA ISLANDS**

STA	DIST	AMP	T	LOG10 (A/MT) + B MB	LOG10 (A/M) + B MB
CU-NV	76.4	24.4	1.20	5.14	5.22
EK-NV	76.5	131.3	1.20	5.87	5.95
RK-ON	95.4	25.0	1.00	5.34	5.34

10 11 12 63 17: 8:12.3 **ALEUTIANS**

STA	DIST	AMP	T	LOG10 (A/MT) + B MB	LOG10 (A/M) + B MB
CU-NV	45.3	20.4	0.50	4.60	4.30
EK-NV	44.9	71.2	1.00	5.24	5.24
RK-ON	50.6	85.0	0.40	5.26	5.06
HN-ME	66.1	151.5	0.80	5.77	5.67

11 19 12 63 20:33:50.1 **ARGENTINA**

STA	DIST	AMP	T	LOG10 (A/MT) + B MB	LOG10 (A/M) + B MB
CU-NV	85.9	66.1	1.20	5.59	5.67
EK-NV	86.4	48.3	1.10	5.41	5.49
RK-ON	88.9	141.0	0.90	5.78	5.74
HN-ME	91.3	109.0	1.10	5.65	5.69

12 12 1 64 6: 0:13.2 **ALEUTIANS**

STA	DIST	AMP	T	LOG10 (A/MT) + B MB	LOG10 (A/M) + B MB
EK-NV	36.8	91.9	1.30	5.41	5.59
CU-NV	37.3	62.0	0.50	4.85	5.03
RK-ON	42.9	154.9	1.10	5.47	5.51
HN-ME	59.3	167.9	0.90	5.65	5.60

13 26 1 64 9: 9:33.9 **PERU**

STA	DIST	AMP	T	LOG10 (A/MT) + B MB	LOG10 (A/M) + B MB
EK-NV	69.0	199.3	0.80	5.80	5.79
CU-NV	68.5	458.7	1.30	6.58	6.70
RK-ON	69.8	684.2	0.50	6.32	6.01
HN-ME	92.5	830.5	0.70	6.42	6.26

14 6 2 64 13: 7:25.2 **ALASKA**

STA	DIST	AMP	T	LOG10 (A/MT) + B MB	LOG10 (A/M) + B MB
EK-NV	31.1	271.6	0.90	5.76	5.71
CU-NV	31.6	160.5	1.00	5.61	5.61
RK-ON	36.2	301.0	1.20	5.91	5.89
HN-ME	52.3	79.2	0.80	5.18	5.09

15 7 2 64 12:58:53.6 **JAPAN**

STA	DIST	AMP	T	LOG10 (A/MT) + B MB	LOG10 (A/M) + B MB
EK-NV	73.4	31.1	1.10	5.14	5.18
CU-NV	73.8	23.7	1.00	4.90	4.90
RK-ON	76.8	63.8	0.90	5.33	5.28

16 8 2 64 11:17:46.5 **ALEUTIANS**

STA	DIST	AMP	T	LOG10 (A/MT) + B MB	LOG10 (A/M) + B MB
RK-NV	47.7	44.3	0.60	5.17	5.12
CU-NV	48.2	15.9	0.40	4.71	4.31
RK-ON	52.6	164.9	0.70	5.46	5.31
HN-ME	67.5	239.4	0.90	6.00	5.96

TABLE VIII (Continued)

Events used and readings at LRSM stations CUNV, EKNV, and RKON.

17 15 1 64 2:23:47.4 **KURILES**

STA	DIST	AMP	T	LOG10(A/MT) + B MB	LOG10(A/M) + B MR
EK-NV	65.5	30.0	1.10	5.26	5.30
CU-NV	66.0	16.5	1.00	4.92	4.92
RK-ON	69.0	91.6	0.90	5.59	5.54

18 15 3 64 22:30:26.0 **GIBRALAR**

STA	DIST	AMP	T	LOG10(A/MT) + B MB	LOG10(A/M) + B MR
EK-NV	79.7	170.8	0.70	5.51	5.35
RK-ON	60.5	482.2	0.80	6.12	6.02
HN-ME	45.4	795.5	0.70	6.18	6.03

19 16 3 64 8:44:32.8 **KURILES**

STA	DIST	AMP	T	LOG10(A/MT) + B MB	LOG10(A/M) + B MR
EK-NV	69.0	80.9	0.90	5.53	5.49
RK-ON	71.0	676.8	0.40	6.36	6.26
HN-ME	54.0	374.9	0.50	6.13	5.93

20 29 3 64 1: 9:36.4 **ALASKA**

STA	DIST	AMP	T	LOG10(A/MT) + B MB	LOG10(A/M) + B MR
EK-NV	29.4	186.9	1.00	5.58	5.58
RK-ON	31.8	385.8	1.20	6.14	6.22
HN-ME	47.4	118.8	1.20	5.83	5.91

21 29 3 64 16:40:57.9 **ALASKA**

STA	DIST	AMP	T	LOG10(A/MT) + B MB	LOG10(A/M) + B MR
EK-NV	28.4	149.2	1.40	5.76	5.90
RK-ON	30.7	291.9	1.10	5.92	5.96
HN-ME	46.4	322.9	1.20	6.21	6.28

22 29 3 64 4:12:15.7 **ALASKA**

STA	DIST	AMP	T	LOG10(A/MT) + B MB	LOG10(A/M) + B MR
EK-NV	28.0	134.6	1.00	5.43	5.43
RK-ON	30.9	279.2	0.90	5.67	5.62
HN-ME	45.5	126.2	1.20	5.71	5.78

23 29 3 64 6: 4:44.5 **KODIAK ISLAND**

STA	DIST	AMP	T	LOG10(A/MT) + B MB	LOG10(A/M) + B MR
EK-NV	30.4	151.5	0.90	5.44	5.40
RK-ON	35.3	118.2	1.30	5.65	5.76
HN-ME	51.4	78.0	1.50	5.63	5.81

24 29 3 64 10: 8: 2.4 **ALASKA**

STA	DIST	AMP	T	LOG10(A/MT) + B MB	LOG10(A/M) + B MR
EK-NV	29.2	76.9	1.20	5.34	5.42
RK-ON	31.5	124.4	1.30	5.72	5.83
HN-ME	47.1	70.5	1.30	5.67	5.78

TABLE VIII (Continued)

Events used and readings at LRSM stations CUNV, EKNV, and RKON.

25 29 3 64 16:45:33.6 ALASKA

STA	DIST	AMP	T	LOG10(A/MT) + B MB	LOG10(A/M) + B MB
EK-NV	28.4	105.4	1.00	5.33	5.33
RK-ON	30.6	130.6	0.90	5.43	5.38
HN-ME	46.3	12.2	0.80	4.50	4.41

26 30 3 64 2:18: 6.3 KODIAK ISLAND

STA	DIST	AMP	T	LOG10(A/MT) + B MB	LOG10(A/M) + B MB
EK-NV	29.8	128.9	1.10	5.49	5.54
RK-ON	34.4	560.5	0.90	6.09	6.05
HN-ME	50.5	94.6	1.10	5.46	5.50

27 30 3 64 13: 3:34.9 KODIAK ISLAND

STA	DIST	AMP	T	LOG10(A/MT) + B MB	LOG10(A/M) + B MB
EK-NV	29.7	137.5	0.80	5.32	5.23
RK-ON	34.3	384.4	0.80	5.87	5.77
HN-ME	50.4	128.7	1.10	5.53	5.63

28 30 3 64 7: 9:34.0 ALASKA

STA	DIST	AMP	T	LOG10(A/MT) + B MB	LOG10(A/M) + B MB
EK-NV	27.9	296.9	1.40	6.05	6.10
RK-ON	30.0	306.5	1.00	5.79	5.79
HN-ME	45.7	215.7	1.20	5.96	6.04

29 30 3 64 15: 7:49.3 ALASKA

STA	DIST	AMP	T	LOG10(A/MT) + B MB	LOG10(A/M) + B MB
EK-NV	29.0	62.5	1.00	5.10	5.10
RK-ON	32.2	216.1	0.80	5.62	5.52
HN-ME	48.0	60.6	0.50	5.24	4.94

30 30 3 64 16: 9:28.4 KODIAK ISLAND

STA	DIST	AMP	T	LOG10(A/MT) + B MB	LOG10(A/M) + B MB
EK-NV	29.4	171.9	1.20	5.69	5.77
RK-ON	34.0	57.9	1.10	5.43	5.47
HN-ME	50.1	68.1	0.90	5.16	5.11

31 31 3 64 0:14:11.7 KODIAK ISLAND

STA	DIST	AMP	T	LOG10(A/MT) + B MB	LOG10(A/M) + B MB
EK-NV	65.3	19.1	1.10	5.06	5.11
RK-ON	68.8	80.0	0.90	5.53	5.48
HN-ME	82.3	114.5	0.90	5.81	5.87

32 31 3 64 9: 1:30.2 VANCOUVER B.C.

STA	DIST	AMP	T	LOG10(A/MT) + B MB		LOG10(A/M) + B MB
EK-NV	15.4	160.8	1.40	5.40	** OMITTED **	5.55
RK-ON	22.8	357.5	1.40	5.92	** OMITTED **	5.96
HN-ME	40.3	206.1	1.00	5.45		5.45

TABLE VIII (Continued)

Events used and readings at LRSM stations CUNV, EKNV, and RKON.

33 4 4 64 4:54: 1.7 ALASKA

STA	DIST	AMP	T	LOG10(A/MT) + B MB	LOG10(A/M) + B MB
EK-NV	28.5	85.5	1.00	5.24	5.24
RK-ON	30.5	307.7	0.90	5.76	5.72
HN-ME	46.1	368.4	1.20	6.23	6.31

34 4 4 64 17:59:43.3 KODIAK ISLAND

STA	DIST	AMP	T	LOG10(A/MT) + B MB	LOG10(A/M) + B MB
EK-NV	30.6	149.0	0.80	5.42	5.32
RK-ON	35.3	179.5	0.90	5.55	5.50
HN-ME	51.4	90.2	0.80	5.24	5.14

35 4 4 64 9:10:55.1 KODIAK ISLAND

STA	DIST	AMP	T	LOG10(A/MT) + B MB	LOG10(A/M) + B MB
EK-NV	29.8	164.5	0.90	5.44	5.39
RK-ON	34.2	487.2	0.70	5.93	5.78
HN-ME	50.3	353.4	0.70	5.78	5.64

36 4 4 64 6:40:29.8 KODIAK ISLAND

STA	DIST	AMP	T	LOG10(A/MT) + B MB	LOG10(A/M) + B MB
EK-NV	29.6	80.6	0.80	5.00	5.00
RK-ON	34.3	251.3	0.90	5.72	5.68
HN-ME	50.4	82.7	0.60	5.15	4.93

37 4 4 64 17:46: 8.6 KODIAK ISLAND

STA	DIST	AMP	T	LOG10(A/MT) + B MB	LOG10(A/M) + B MB
EK-NV	30.5	123.0	0.80	5.33	5.23
RK-ON	35.3	371.8	0.90	5.86	5.82
HN-ME	51.4	342.1	1.10	6.02	6.06

38 3 4 64 8:38:42.8 ALASKA

STA	DIST	AMP	T	LOG10(A/MT) + B MB	LOG10(A/M) + B MB
EK-NV	27.3	85.9	1.20	5.32	5.40
RK-ON	29.6	120.5	1.10	5.46	5.51
HN-ME	45.3	155.3	1.30	5.84	5.96

39 3 4 64 8:46:26.9 ALASKA

STA	DIST	AMP	T	LOG10(A/MT) + B MB	LOG10(A/M) + B MB
EK-NV	29.1	69.5	1.20	5.30	5.38
RK-ON	32.8	56.4	0.80	5.04	4.94
HN-ME	48.6	68.2	1.20	5.51	5.50

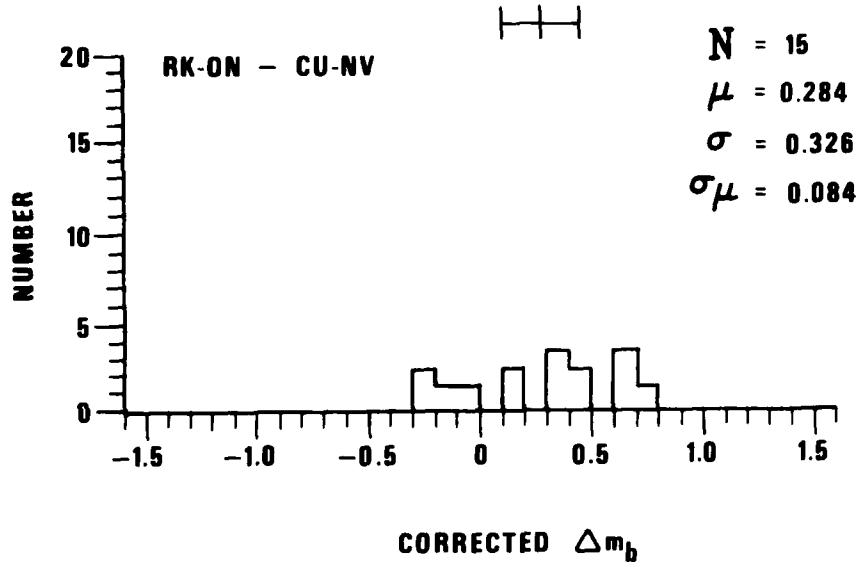

Figure 48. Histogram of magnitude differentials between stations RKON and CUNV.

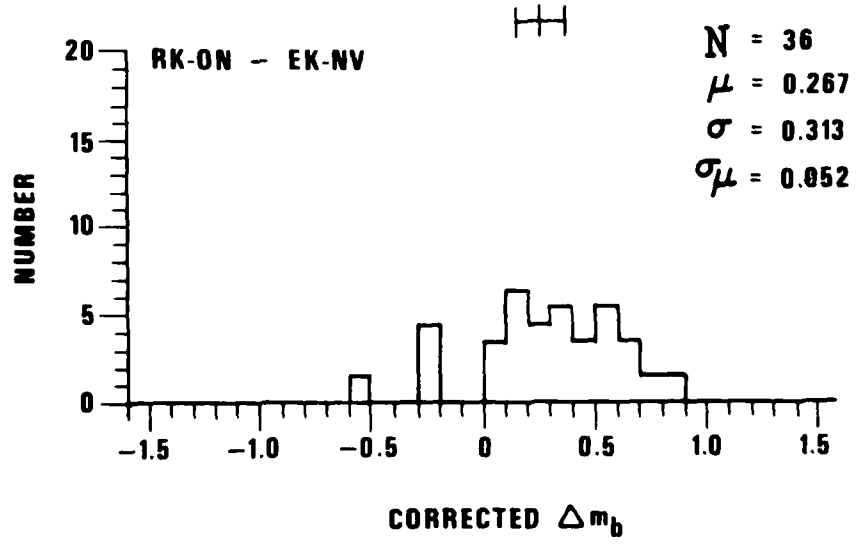

Figure 49. Histogram of magnitude differentials between stations RKON and EKNV.

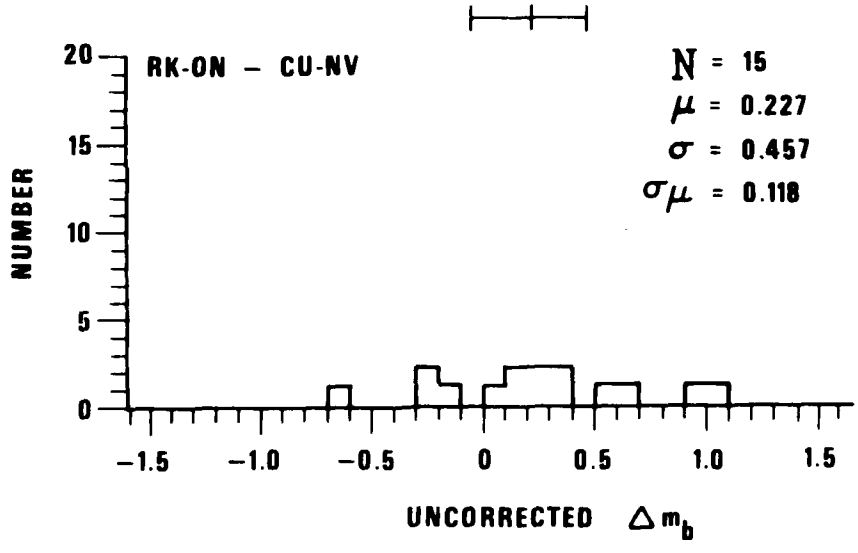

Figure 50. Histogram of uncorrected magnitude differentials between stations RKON and CUNV.

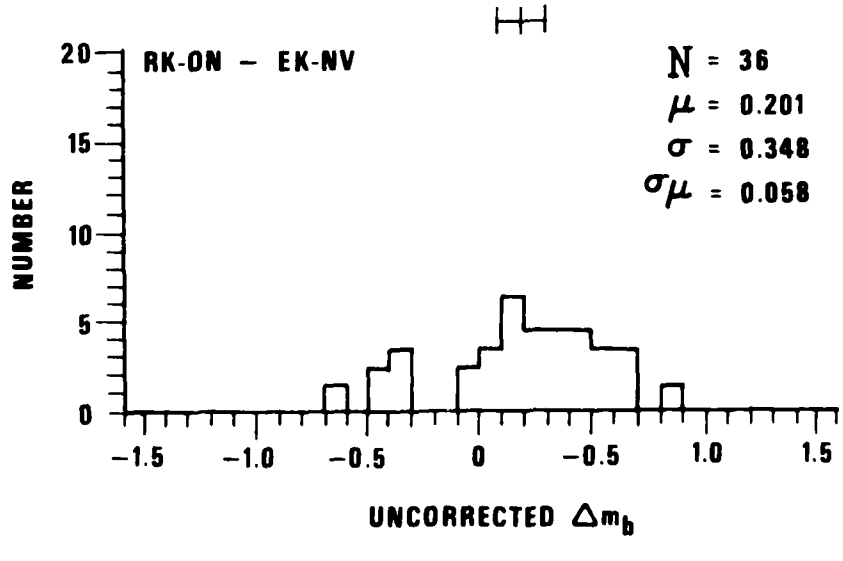

Figure 51. Histogram of uncorrected magnitude differentials between stations RKON and EKNV.

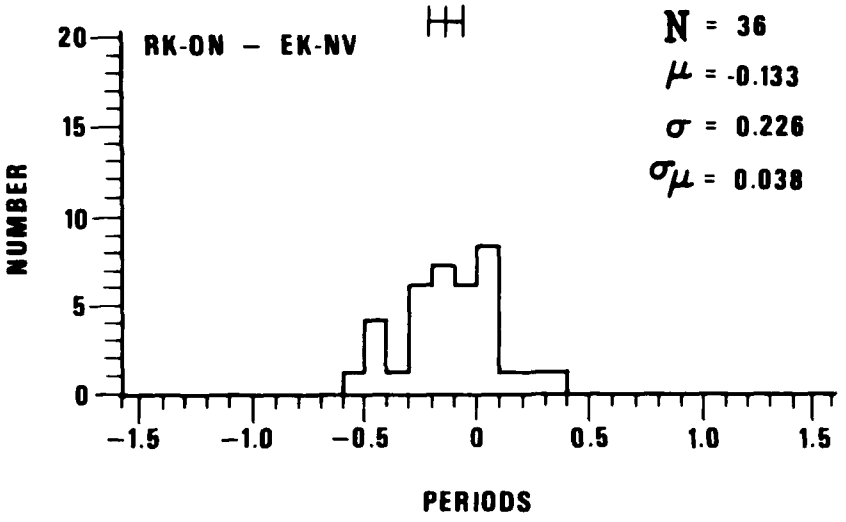

Figure 52. Histogram of P wave period differentials for the station pair RKON-EKNV.

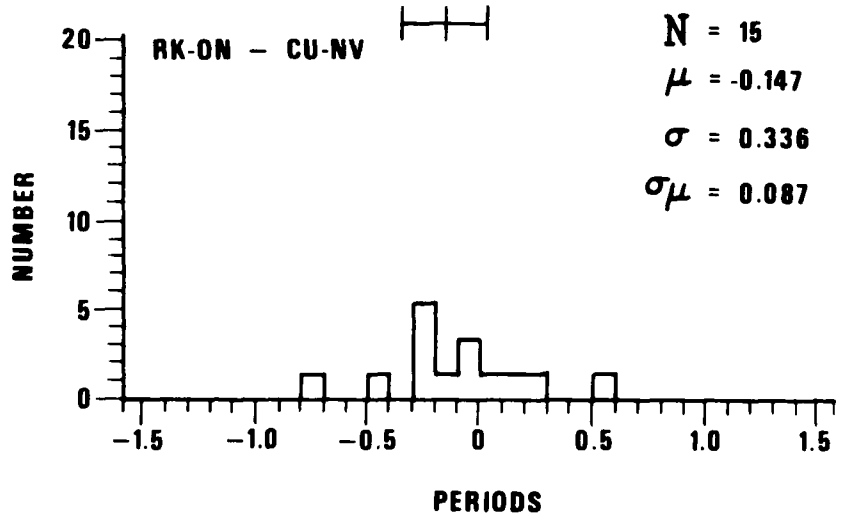

Figure 53. Histogram of P wave period differentials for the station pair RKON-CUNV.

the significance of this result is lower than 95% with the sample size (only 15 events) available. Attempts to determine magnitude differentials at other LRSM stations near NTS were not successful due either to the short operational life of these stations or to difficulties in reading films without proper time marks. In summary, the results demonstrate that both EKNV and CUNV have negative magnitude station effects relative to RKON, thus conforming to the general pattern of WUS stations and indicating higher attenuation under WUS. North (1976) also showed that EKNV has a magnitude residual relative to EUS that is comparable to those of other stations in the Basin and Range. Both EKNV and CUNV are on well-consolidated sediments so that they might be expected to have slightly higher amplitudes than a station on granite nearby.

General Limitations of the Values of t*

Much disagreement still exists in seismological literature concerning the proper value of t* for short-period waves. While some investigators use values as high as 1.15 for WUS-shield paths, others have pointed out that losses along shield-to-shield paths are small (Douglas et al., 1974), corresponding to a t* of about .2. Still others have reported that attenuation along certain shield-to-shield paths is not measurable (Filson, personal communication), which corresponds to t* $\sim$ 0. These assertions cannot both be true, because taking the difference of WUS-shield and shield-to-shield t* values gives a t* $\sim$ 1, resulting in a huge magnitude differential (about 1.5 magnitude units at 1 Hz) between the two types of paths. This is clearly in conflict with the observations.

Most discrepancies among these results are due to assumptions about the source spectra used to determine absolute values of t*. In reality, the most unreliable way to estimate t* is time-domain waveform matching. While possibly a good visual agreement can be obtained between observed and synthetic short-period seismograms using only the relatively low-frequency components (f < 1.5 Hz) or the spectrum, if the corner frequency is below 1.5 Hz and ignoring

---

Douglas, A., J. A. Hudson, P. D. Marshall, and J. B. Young (1974). Earthquakes that look like explosions, Geophys. J. R. Astr. Soc., 36, 227-233.

discrepancies at higher frequencies which determine t*, even this crude procedure rules out t* $\sim$ 1 in most cases (Somerville et al., 1976). A still more suspect procedure is to match only the amplitudes of the first few cycles of the synthetics to the observed waveforms. This method brings into play a whole set of unknown factors, such as the upper mantle structure, crustal structure, etc., and the effect of t* becomes inseparable from all of the other factors.

If analysis of t* is performed in the frequency domain, then the range of allowable t* is clearly limited by both the data and the level of knowledge of seismic sources. Thus, discussions here are confined to large events (m_b > 5) because spectra of such events are better characterized in the short-period band (.5-4. Hz). Large nuclear explosions have a corner frequency of around 1 Hz, and the theoretical spectrum above this frequency varies as ω^{-2} (von Seggern and Blandford, 1972; Mueller and Murphy, 1971). This estimate is in agreement with spectra derived from reduced displacement potentials used here for determining t* (Der and McElfresh, 1975). Assuming greater slopes (Haskell, 1964) would lead to extremely low or even negative t* values, thus contradicting any large t*. Peppin's (1977) suggestion of an ω^{-4} fall-off rate for explosions in tuff is not relevant to this discussion because only explosions in hard rock or salt were used to determine t*.

This situation also exists for earthquakes because there is no indication that spectral slopes for large earthquakes are less than ω^{-2} (Brune, 1970).

Peppin, W. A. (1977). A near-regional explosion source model for tuff, Geophys. J. R. Astr. Soc., 48, 331-350.

Brune, J. N. (1970). Tectonic stress and the spectra of seismic shear waves from earthquakes, J. Geophys. Res., 75, 4997-5009.

Somerville, P. G., R. A. Wiggins, and R. M. Ellis (1976). Time domain determination of earthquake fault parameters from short-period P waves, Bull. Seism. Soc. Am., 66, 1459-1484.

Mueller, R. A. and J. R. Murphy (1971). Seismic characteristics of underground nuclear detonations, Bull. Seism. Soc. Am., 61, 1965.

Haskell, N. A. (1964). Radiation pattern of surface waves from point sources in multi-layered mediums, Bull. Seism. Soc. Am., 54, 377-393.

On the contrary, both theoretical considerations and observational data indicated that the fall-off rate may be closer to ω^{-3} (Geller, 1976; von Seggern and Blandford, 1972). Computing spectral ratios by utilizing source spectra with either ω^{-2} or ω^{-3} fall-off rates will give t* values considerably less than unity (Noponen, 1975; von Seggern and Sobel, 1976; Sobel, von Seggern, Sweetser and Rivers, 1977a,b,c) in agreement with t* determinations from nuclear explosions.

Smaller explosions and earthquakes can have overall slopes of less than ω^{-2} in the short-period band, but in all cases where the spectrum has been determined (from close-in measurements for instance) analysis yields t* values of the same magnitude as already existing studies which used only large high frequency fall-off rates.

Variability of t* Measurements

While Δt^* measurements appear to behave consistently for given types of source-receiver pairs, it is important to have some idea of the magnitude of scatter expected for such measurements. One factor causing the drastic variation in body-wave amplitudes is multipathing, and this same factor will,

---

Geller, R. J. (1976). Scaling relations for earthquake source parameters and magnitudes, Bull, Seism. Soc. Am., 66, 1501-1523.

Noponen, I. (1975). Compressional wave power spectrum from seismic sources, Institute of Seismology, University of Helsinki, ISNB-951-45-0538, Contract, AFOSR-72, 2377, Final Report.

von Seggern, D. and P. Sobel (1976). Study of selected Kamchatka earthquakes in a seismic discrimination context, SDAC-TR-76-10, Teledyne Geotech, Alexandria, Virginia 22314.

Sobel, P. A., D. H. von Seggern, E. I. Sweetser, and D. W. Rivers (1977a). Study of selected events in the Baikal Rift Zone in a seismic discrimination context, In preparation.

Sobel, P. A., D. H. von Seggern, E. I. Sweetser, and D. W. Rivers (1977b). Study of selected events in the Caucasus in a seismic discrimination context, In preparation.

Sobel, P. A., D. H. von Seggern, E. I. Sweetser, and D. W. Rivers (1977c). Study of selected events in the Pamirs in a seismic discrimination context, SDAC-TR-77-3, Teledyne Geotech, Alexandria, Virginia 22314.

undoubtedly, cause variations in the spectra which can influence Δt^* measurements. To determine the range of the spectra variation within a relatively small area, the spectra of P waves were computed on a single sensor of each subarray of NORSAR. (The events were taken from Blandford's [1974] report because they were conveniently available on digital tapes.) The maximum variation of P wave amplitudes among subarrays was about five to one, indicating considerable multipathing and site effects. If the area occupied by NORSAR is considered a typical piece of the Earth's crust, the variability of Δt^* can be assessed by taking ratios of these spectra. The reference spectrum used was the average of spectra at all sensors for each individual event. Individual sensor spectra were divided by this average and straight lines were fitted to the ratios to determine apparent Δt^* values. Since no real variations of t^* were expected across NORSAR, and since all stations are on hard rock the scatter of these values is thought to be a result of multipathing across the array. The procedures used to compute the spectra and the ratios are identical to those utilized for computing our other t^* values.

Epicentral data for analyzed events are given in Table IX, and the Δt^* values at various subarrays are given in Table X. A histogram of all Δt^* values is given in Figure 54. The standard deviation of these values is small, $\sigma_{t^*} = .063$, giving a 95% limit of a single t^* measurement of $\pm.13$. Thus, assuming this scatter typical for general t^* measurements that are used in establishing a regional difference in t^* for the shield-to-shield and shield-to-WUS paths only a few pairs of measurements should suffice, but individual measurements can still considerably overlap. On the other hand, a much larger number of amplitude measurements is needed to establish a magnitude station bias for a pair of stations. These facts are quite obvious from the above results for both Δt^* and Δm_b.

Blandford, R. R. (1974). Short-period signal-to-noise ratio at NORSAR, SDAC-TR-74-13, Teledyne Geotech, Alexandria, Virginia 22314.

TABLE IX

Events Used to Determine Δt* Values at NORSAR

EVENT	DATE	ORIGIN	LAT.	LONG.	M_b	Δ	Az	DEPTH	TAPE	SUBSET TAPE
KAZ 145 04N	5-25-71	04:02:57	49.8N	78.2E	5.2	38.0	75.4	0	13034	L07292
RYU 240 15N	8-28-71	15:57:48	28.3N	130.7E	5.7	78.5	51.2	35	15282	L08589
URA 191 16N	7-10-71	16:59:59	64.2N	55.2E	5.3	20.3	61.2	0	11095	L03502
IRA 221 02N	8-09-71	02:54:37	36.2N	52.7E	5.2	36.0	113.7	27	10227	L08296
TIB 123 00N	5-03-71	00:33:22	30.8N	84.5E	5.4	55.6	87.3	16	13261	L06401
KUR 213 02N	8-01-71	02:06:06	50.4N	156.8E	5.6	65.5	23.1	20	07181	L06583
SIN 207 01N	7-26-71	01:48:33	39.9N	77.2E	6.0	44.8	86.4	20	13336	L08276

TABLE X

Summary of Δt^* Values Computed at NORSAR

EVENT

SUB ARRAY	KAZ 145	RYU 240	URA 191	IRA 221	TIB 123	KUR 213	SIN 207
01A	.052	.077	.066	.155	-.067	-.007	-.004
01B	-.089	-.030	-.037	-.032	.092	-.079	.031
02B	-.055	.009	.028	.071	.035	.026	-.033
03B	-.022	.036	.110	.024	.026	-.012	-.090
04B	.005	-.018	.022	.025	.020	.061	.065
05B	.169	-.011	.004	-.079	-.025	.055	-.061
06B	.037	.036	-.054	-.059	-.010	.104	.035
07B	-.029	.037	.056	.031	-.063	.054	.151
02C	.041	-.034	.016	.091	.061	.093	.074
03C	.051	-.072	.075	.006	-.084	-.072	.167
04C	.045	-.035	-.024	.114	.151	.007	.020
05C	.015	.068	.006	.170	.090	-.008	-.045
06C	-.011	.024	-.008	-.077	-.015	-.111	.054
07C	.014	.009	-.167	-.004	.017	-.010	.096
08C	.122	.019	-.016	-.047	-.008	.071	-.012
09C		.051	.003	.051	.058	.077	.083
10C		.073		-.009	.093	-.031	.093
11C		.062		.056	.028	.025	.058
12C		-.057		.069	.059	.077	.128
13C		.071		.017	.081		.003
14C		.174		.126	-.064		.046

N = 139
MEAN = .024
STD. DEV. = .063

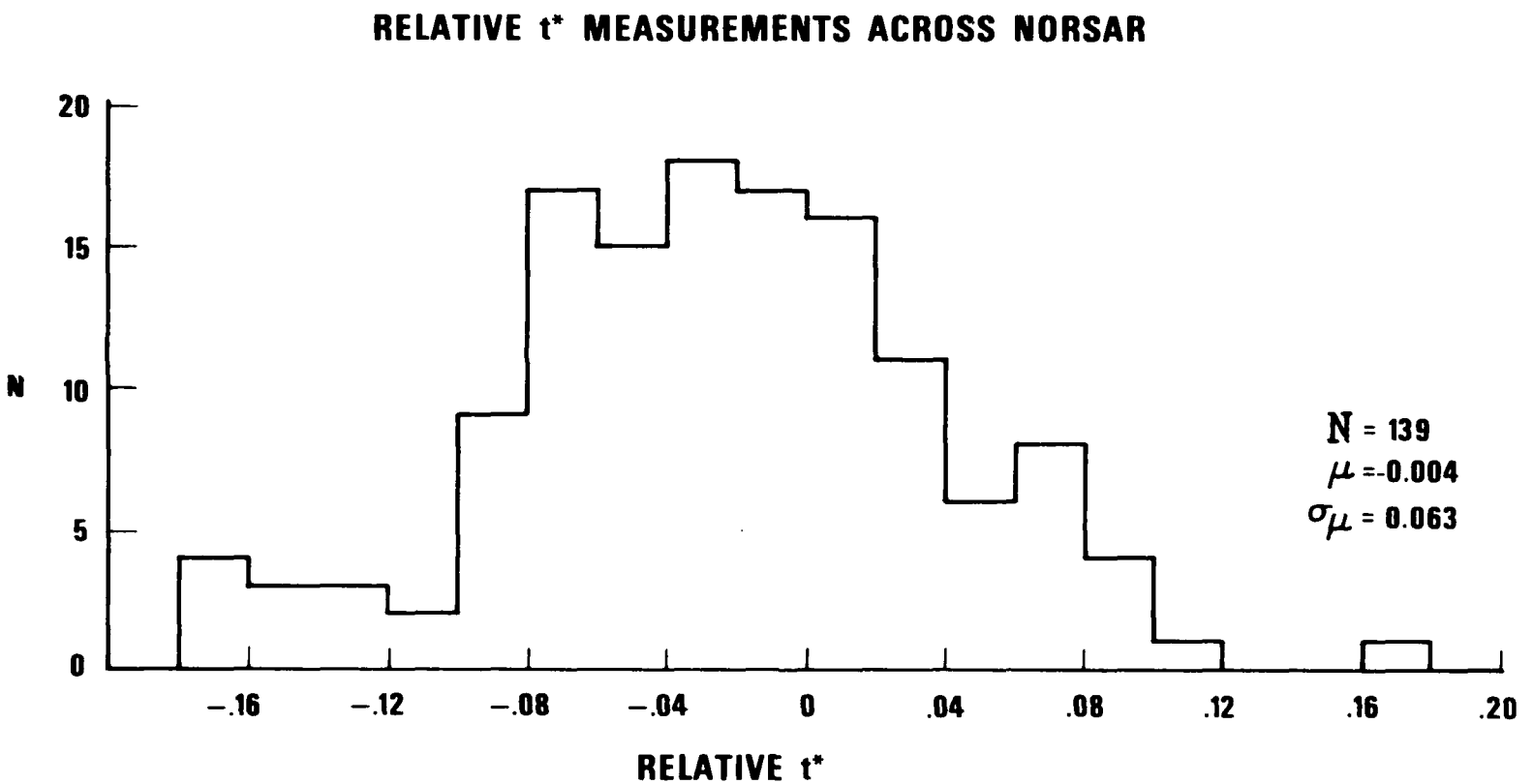

Figure 54. Histogram of Δt^* values between various subarrays of NORSAR.

DISCUSSION OF RESULTS

The purpose of this study is the evaluation of attenuation under NTS. Attenuation is the only truly reciprocal factor with respect to source-receiver postions. There is an additional problem for a nuclear explosion source: reciprocity does not hold because the equivalent elastic source changes with shot medium, even if reciprocity would be strictly valid for the same equivalent elastic sources.

Evaluating attenuation characteristics using teleseismic P waves is a difficult task, utilizing several basic assumptions that cannot always be easily substantiated. The difficulty lies in deciding which observed anomalies are reciprocal with respect to interchange of sources and receivers. Ideally, a station located over an attenuating upper mantle should show lower amplitudes for teleseismic waves than a station with less attenuation underneath, and their spectral ratios should show the degree of differential attenuation. Crustal structure, however, can change the absolute level of P wave amplitudes, especially if the surface is covered with low-velocity materials. While crustal structure can also change the slopes of spectral ratios, our calculations using a large number of crustal LRSM station responses show that in most cases the slopes do not change significantly in the total frequency band (.5-5. Hz) even if the absolute levels of P wave amplitudes are modified significantly by the receiver structure. A similar argument can be used for the effects of systematic crustal focusing or defocusing: multipathing could probably be compensated for by using many events at various azimuths and distances. In addition, the possibility exists that at some individual stations the crustal response might significantly change the shape of observed body-wave spectra so that t* cannot be reliably measured. Still, the spectral ratio measurements remain more reliable diagnostics of attenuation and thus of the expected effect on m_b from sources at the station site than are absolute amplitudes.

Measuring attenuation under individual stations is more difficult than measuring regional attenuation patterns because (Der, 1976; Der and McElfresh, [illegible]) regional studies average over many stations and tend to minimize the [illegible] local crustal distortion of amplitudes and spectra at individual

An apparent discrepancy exists between the sizes of magnitude and amplitude differentials at RKON and OB2NV on one hand and, on the other hand, the size of $\Delta t^* \sim .17$. This is possibly due to crustal focussing at NTS. The magnitude differential is significantly less than predicted by the amplitude attenuation factor computed for a single frequency (1 Hz was commonly used in previous studies).

The magnitudes are also significantly lower by a similar amount at NTNV and NT2NV relative to RKON, if the .2 magnitude unit correction for parallel layer crustal effects mentioned above is made. This correction assumes that the crust and the upper mantle under the volcanics at Pahute Mesa and Climax Stock are the same, which may not be true.

Based upon measurements of dominant P wave period differentials between EUS and WUS (.1-.2 sec), it is unlikely that the previously reported EUS-WUS magnitude differentials (Booth, Marshall and Young, 1974) can be attributed solely to changes in period. Even if a .1 magnitude unit (maximum) difference is assumed as result of the period differential, the remainder must be due to differences in absolute amplitude.

The study of SHOAL and the comparison of SZNV and SEMN indicates that the mantle under SHOAL is typical of the WUS both in the EUS-WUS differential Δt^* and in the absolute values of t^* for SHOAL-to-shield type paths. The magnitude bias at the SHOAL site has been shown to be not significantly different from MNNV (Der and McElfresh, 1976), which had a bias of $-.28 \pm .05$ relative to global averages of m_b (Booth, Marshall and Young, 1974).

The study of CUNV and EKNV shows that these stations are also typical of WUS with significantly lower magnitudes and larger P wave periods than EUS stations.

This study firmly establishes that short-period P waves, crossing the upper mantle under the Basin and Range province, lose a great portion of their high-frequency energy relative to those travelling under shields. The number of spectral measurements presented here is greater than in any similar data set previously published. The differences in spectral content are statistically significant on at least the 95% confidence level.

There seems to be the possibility that at individual stations the measured magnitude bias of incoming teleseismic waves is significantly modified at NTS by crustal structure resulting in focussing. Such modification is not in general reciprocal with respect to exchange of source-receiver positions, while the effect of attenuation is reciprocal.

The spectral ratio results presented in this report fit well into the framework of previous studies of t* in shield regions versus shield-WUS type paths. Figure 55 shows a compilation of t* calculations plotted against epicentral distance previously presented in Seismic Data Analysis Center Technical Report 76-8 with some new data points added. On the right of the figure we show the EUS-WUS coverage differential in t* for some Novaya Zemlya shots and for the two station pairs SEMN-SZNV and OB2NV-RKON presented in this report. The differentials in t* are roughly equal to differences between the absolute t* determinations at teleseismic distances. Thus, within the limits of accuracy of the present measurements, the NTS stations behave as typical WUS stations with respect to t*.

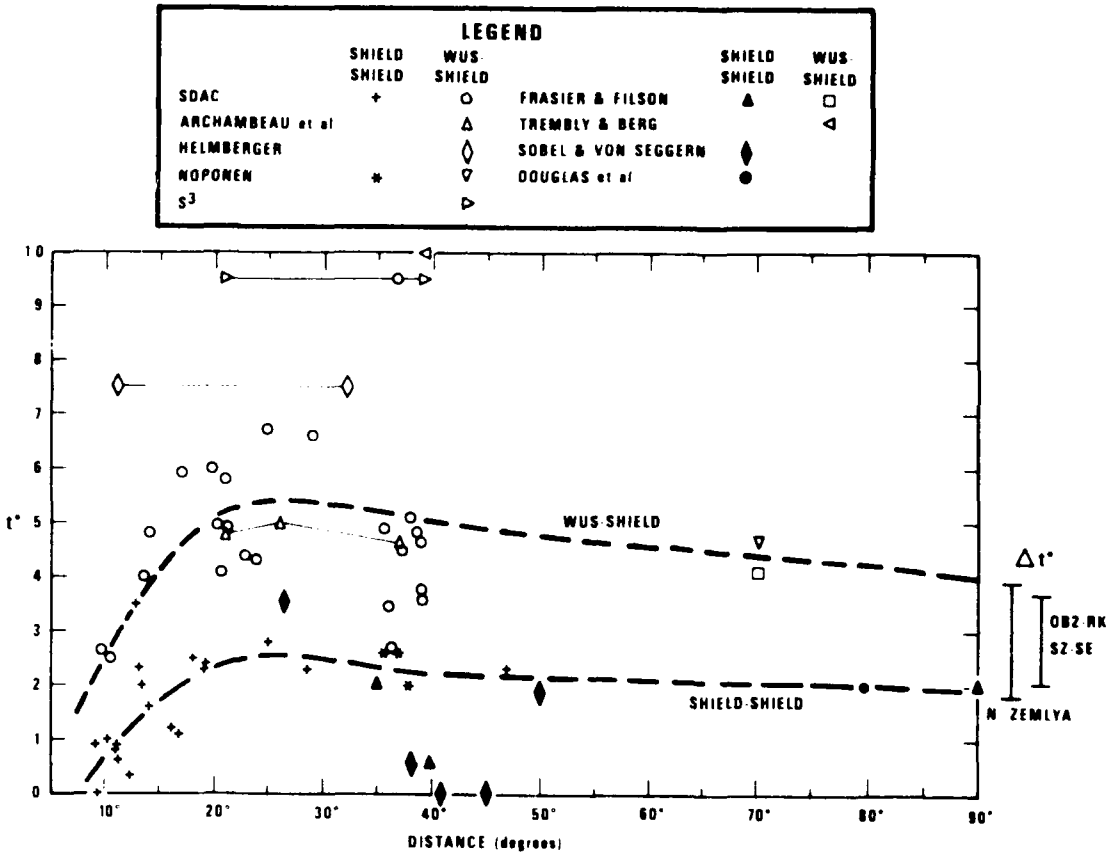

Figure 55. Summary of available t* calculations vs. epicentral distance.

ACKNOWLEDGEMENTS

Several people besides the authors of this report made significant contributions to this study. The data services group under J. R. Woolson provided a considerable amount of data. Discussions with USAF Captain Gregory B. Young led to the resolution of an apparent discrepancy between Δt^* and Δm_b at OB2NV. Mr. Brian W. Barker did the relative t* study at NORSAR.

REFERENCES

Blandford, R. R. (1974). Short-period signal-to-noise ratio at NORSAR, SDAC-TR-74-13, Teledyne Geotech, Alexandria, Virginia, 22314. ADA 015350

Blandford, R. R. (1976). Experimental determination of scaling laws for contained and cratering explosions, Seismic Data Analysis Center, SDAC-TR-76-3, Teledyne Geotech, Alexandria, Virginia, 22314. ADA 03635

Blandford, R. R. and Z. A Der (1977). Gross characteristics of short-period seismic P waveforms from nuclear explosions as functions of source type, medium, instruments, attenuation, and burial depth. SDAC technical report in preparation. Teledyne Geotech, Alexandria, Virginia, 22314.

Booth, D. C., P. D. Marshall, and J. B. Young (1974). Long- and short-period amplitudes from earthquakes in the range 0°-114°, Geophys. J. R. Astr. Soc., 39, 523-538.

Brune, J. N. (1970). Tectonic stress and the spectra of seismic shear waves from earthquakes, J. Geophys. Res., 75, 4997-5009.

Der, Z. A. (1976). On the existence, magnitude and causes of broad regional variations in body-wave amplitudes (magnitude bias), SDAC-TR-76-8, Teledyne Geotech, Alexandria, Virginia, 22314.

Der, Z. A., R. P. Massé, and J. P. Gurski (1975). Regional attenuation of short-period P and S waves in the United States, Geophys. J. R. Astr. Soc., 40, 85-106.

Der, Z. A. and T. W. McElfresh (1975). Short-period P wave attenuation along various paths in North America as determined from P wave spectra of the SALMON nuclear explosion, SDAC-TR-75-16, Teledyne Geotech, Alexandria, Virginia, 22314. ADA 025239

Der, Z. A. and T. W. McElfresh (1976a). Short-period P wave attenuation along various paths in North America as determined from P wave spectra of the SALMON nuclear explosion, Bull. Seism. Soc. Am., 66, 1609-1622.

Der, Z. A. and T. W. McElfresh (1976b). The effect of attenuation on the spectra of P waves from nuclear explosions in North America, SDAC-TR-76-7, Teledyne Geotech, Alexandria, Virginia, 22314. ADA 030857

Der, Z. A. and T. W. McElfresh (1977). The relationship between anelastic attenuation and regional amplitude anomalies of short-period P waves in North America, Bull. Seism. Soc. Am., 67, No. 5, 1303-1317.

Douglas, A., J. A. Hudson, P. D. Marshall, and J. B. Young (1974). Earthquakes that look like explosions, Geophys. J. R. Astr. Soc., 36, 227-233.

Evernden, J. and D. M. Clark (1970). Study of teleseismic P. II. Amplitude data, Phys. Earth. Planet Int., 4, 24-31.

Geller, R. J. (1976). Scaling relations for earthquake source parameters and amplitudes, Bull. Seism. Soc. Am., 66, 1501-1523.

Gutenberg, B. and C. F. Richter (1956). Magnitude and energy of earthquakes, Ann Geof. (Rome), 9, 1-15.

Guyton, J. W. (1964). Systematic deviations of magnitude from body-waves at seismograph stations in the United States. Proceedings of VESIAC Conference on Seismic Event Magnitude Determination, University of Michigan, 4410-71-X.

Haskell, N. A. (1967). Radiation pattern of surface waves from sources in multi-layered mediums, Bull. Seism. Soc. Am., 54, 377-393.

Herrin, E. and W. Tucker (1972). On the estimation of body-wave magnitudes, Report to AFOSR, Dallas Geophysical Observatory, Southern Methodist University, Dallas, Texas.

Hoel, P. G. (1954). Introduction to Mathematical Statistics: New York, John Wiley & Sons.

Mueller, R. A. and J. R. Murphy (1971). Seismic characteristics of underground nuclear detonations, Bull. Seism. Soc. Am., 61, 1675.

Noponen, I. (1975). Compressional wave power spectrum from seismic sources, Institute of Seismology, University of Helsinki, ISNB-45-0538, Contract AFOSR-72, 2377, Final Report.

North, R. G. (1976). Station biases in body-wave magnitude (abstract), Transactions, American Geophysical Union (E⊕S), 57, 955.

Peppin, W. A. (1977). A near-regional explosion source model for tuff, Geophys. J. R. Astr. Soc., 48, 331-350.

Sobel, P. A., D. H. von Seggern, E. I Sweetser, and D. W. Rivers (1977a). Study of selected events in the Baikal Rift Zone in a seismic discrimination context, In preparation.

Sobel, P. A., D. H. von Seggern, E. I. Sweetser, and D. W. Rivers (1977b). Study of selected events in the Caucasus in a seismic discrimination context, In preparation.

Sobel, P. A., D. H. von Seggern, E. I. Sweetser, and D. W. Rivers (1977c). Study of selected events in the Pamirs in a seismic discrimination context, SDAC-TR-77-3, Teledyne Geotech, Alexandria, Virginia, 22314.

Solomon, S. C. and M. N. Toksöz (1970). Lateral variation of attenuation of P and S waves beneath the United States, Bull. Seism. Soc. Am., 60, 819-838.

Somerville, P. G., R. A. Wiggins, and R. M. Ellis (1976). Time domain determination of earthquake fault parameters from short-period P waves, Bull. Seism. Soc. Am., 66, 1459-1484.

Spence, W. (1974). P wave residual differences and inferences on an upper mantle source for the Silent Canyon Volcanic Centre, Southern Great Basin, Nevada, Geophys. J. R. Astr. Soc., 38, 505-523.

von Seggern, D. H. and R. R. Blandford (1972). Source-time functions and spectra for underground nuclear explosions, Geophys. J. R. Astr. Soc., 31, 89-97.

von Seggern, D. H. and R. R. Blandford (1976a). Seismic threshold determination, Bull. Seism. Soc. Am., 66, 753-788.

von Seggern, D. H. and R. R. Blandford (1976b). Observed variation in the spectral discriminant from short-period P waves, SDAC-TR-76-12, Teledyne Geotech, Alexandria, Virginia, 22314.

von Seggern, D. H. and P. A. Sobel (1976). Study of selected Kamchatka earthquakes in a seismic discrimination context, SDAC-TR-76-10, Teledyne Geotech, Alexandria, Virginia, 22314.

Walsh, J. B. (1968). Attenuation in partially melted material, J. Geophys. Res., 73, 2209-2216.

Walsh, J. B. (1969). New analysis of attenuation in partially melted rock, J. Geophys. Res., 74, 4333-4337.